REPORT SERIES IN AEROSOL SCIENCE
N:o 225 (2019)

CHARACTERIZING ORGANIC AEROSOL PROPERTIES THROUGH PROCESS MODELLING

OLLI-PEKKA TIKKANEN

Department of Applied Physics
Faculty of Science and Forestry
University of Eastern Finland
Kuopio, Finland

Academic dissertation

To be presented, with the permission of the Faculty of Science and Forestry of the University of Eastern Finland, for public criticism in auditorium SN200, Yliopistonranta 1, on December 17th, 2019 at 12 o'clock noon.

Kuopio 2019

Author's Address: Department of Applied Physics
P.O. Box 1627
FI-70211 University of Eastern Finland
optikkanen@gmail.com

Supervisors: Associate Professor Taina Yli-Juuti, Ph.D.
Department of Applied Physics
University of Eastern Finland

Professor Kari Lehtinen, Ph.D.
Department of Applied Physics
University of Eastern Finland

Docent Santtu Mikkonen, Ph.D.
Department of Applied Physics
University of Eastern Finland

Reviewers: Professor Miikka Dal Maso, Ph.D.
Physics unit
Faculty of Engineering and Natural Sciences
Tampere University

Docent Tomi Raatikainen, Ph.D.
Finnish Meteorological Institute
Helsinki, Finland

Opponent: Reader David Topping, Ph.D.
Department of Earth and Environmental Sciences
University of Manchester, UK

ISBN 978-952-7276-32-7 (printed version)
ISSN 0784-3496
Helsinki 2019
Unigrafia Oy

ISBN 978-952-7276-33-4 (pdf version)
http://www.atm.helsinki.fi/FAAR/
Helsinki 2019

Acknowledgements

The research presented in this thesis was carried out in the Department of Applied Physics of the University of the Eastern Finland, Kuopio. I want to thank the Head of the Department Prof. Kari Lehtinen and the Head of the Aerosol Physics group Prof. Annele Virtanen for providing me with the working facilities and for creating such an inspiring atmosphere.

My sincerest gratitude goes towards my excellent supervisors Assoc. Prof. Taina Yli-Juuti, Prof. Kari Lehtinen and Dr. Santtu Mikkonen for teaching me how to do science and for expressing interest towards my work, ideas and well-being. Above all, I want to thank my principal supervisor Assoc. Prof. Taina Yli-Juuti who has guided me since my B.Sc. studies and who has always had time for me and my questions. Thank you for all the years.

I thank Prof. Miikka Dal Maso and Dr. Tomi Raatikainen for reviewing this thesis.

I express my gratitude towards all the co-authors who have contributed to this thesis. Special thanks go to Dr. Angela Buchholz for showing me the experimental side of the aerosol science and for always being ready to answer my questions about experiments or how to interpret experimental data. Prof. Jonathan P. Reid, Dr. Grazia Rovelli and Dr. Antti Lipponen are also acknowledged for the fruitful collaboration. I thank Olli Väisänen and Zijun Li for being excellent co-authors and colleagues. Thanks go also to Sini Isokääntä and Eemeli Holopainen for being such great office mates.

I have truly enjoyed working in Kuopio and will miss the whole research group as well as the daily coffee breaks. Keep up the good work!

I want to thank all my friends and family without whom life would not be whole. Thanks to each and everyone of you. You have a special place in my heart! Finally, I thank Aino for sharing this life with me.

Olli-Pekka Tikkanen
University of Eastern Finland, 2019

Abstract

An aerosol is a colloidal system consisting of particles in a solid or liquid state and of a gas that surrounds the particles. The aerosol particles have important effects on our health via the air we breathe as well as its visibility visibility and also on the climate.

Aerosol particles can be directly emitted to the atmosphere, but they are also formed when atmospheric trace gases, such as sulfuric acid, ammonia, amines, various organic compounds and water nucleate to form nanometer-sized clusters. The growth dynamics of these clusters towards sizes where their effects on the climate are determined by condensation of available vapors and the coagulation of particles with each other.

The volatile organic compounds (VOC), such as α-pinene, are a significant source of condensable vapor. VOCs become oxidized in the atmosphere to form organic compounds that can partition into the particles. The two key quantities related to understanding the dynamics of organic aerosol (OA) are 1) the volatility of the organic compounds and 2) the viscosity in the particle phase. These are also properties that are challenging to measure directly. This thesis presents and validates an alternative way to estimate both volatility and viscosity from isothermal particle evaporation experiments by using process modelling and global optimization methods. The validation was performed by using both modelled and experimentally measured OA evaporation data: these showed that in the majority of the studied cases, the method produces reliable estimates for the studied properties.

The process model optimization method was used to estimate the volatility and viscosity of α-pinene SOA, i.e., secondary organic aerosol formed from the oxidation products of α-pinene. A significant fraction of organic compounds with low volatility were needed to explain the measured particle evaporation rates. A strong composition dependent viscosity was needed to explain the evaporation dynamics in low relative humidity conditions. In most atmospheric conditions near the surface of the earth, it was found that volatility was the most important property for determining the SOA dynamics.

The ability of a state-of-the-art thermodynamic model to estimate the hygroscopicity, i.e, the water uptake, of particles containing sulfuric acid, ammonia and dimethylamine (DMA) was studied also in this thesis. The results revealed that the model underestimated the hygroscopicity of DMA-containing particles when the particle size was in the order of a few tens of nanometers prompting a need for further studies to clarify the thermodynamics of DMA-containing solutions.

Keywords: SOA, volatility, viscosity, hygroscopicity

Contents

List of publications

This thesis consists of an introductory review, followed by five research articles. In the introductory part, these papers are cited according to their roman numerals. **Papers I–II** are reprinted under the Creative Commons Attribution 4.0 License. **Paper III** under the Creative Commons Attribution-NonCommercial-NoDerivs 4.0 License and **Papers IV–V** under a license obtained from the publisher.

I **Tikkanen, O.-P.**, Hämäläinen, V., Rovelli, G., Lipponen, A., Shiraiwa, M., Reid, J. P., Lehtinen, K. E. J., and Yli-Juuti, T.: Optimization of process models for determining volatility distribution and viscosity of organic aerosols from isothermal particle evaporation data, *Atmospheric Chemistry and Physics*, 19, 9333–9350, https://doi.org/10.5194/acp-19-9333-2019, 2019.

II **Tikkanen, O.-P.**, Buchholz, A., Ylisirniö, A., Schobesberger, S., Virtanen, A., and Yli-Juuti, T.: Comparing SOA volatility distributions derived from isothermal SOA particle evaporation data and FIGAERO-CIMS measurements, *Atmospheric Chemistry and Physiscs Discussions*, https://doi.org/10.5194/acp-2019-927, in review, 2019.

III Yli-Juuti, T., Pajunoja, A., **Tikkanen, O.-P.**, Buchholz, A., Faiola, C., Väisänen, O., Hao, L., Kari, E., Peräkylä, O., Garmash, O., Shiraiwa, M., Ehn, M., Lehtinen K.E.J., and Virtanen A.: Factors controlling the evaporation of secondary organic aerosol from α-pinene ozonolysis, *Geophysical research letters*, 44(5), 2562–2570, https://doi.org/10.1002/2016GL072364, 2017

IV Li, Z., **Tikkanen, O.-P.**, Buchholz, A., Hao, L., Kari, E., Yli-Juuti, T., and Virtanen, A.: Effect of Decreased Temperature on the Evaporation of α-Pinene Secondary Organic Aerosol Particles, accepted to *ACS Earth and Space Chemistry*, https://doi.org/10.1021/acsearthspacechem.9b00240, 2019

V **Tikkanen, O,-P.**, Väisänen, O., Hao, L., Holopainen, E., Wang, H., Lehtinen, K.E.J., Virtanen A., and Yli-Juuti, T.: Hygroscopicity of dimethylaminium-, sulfate-, and ammonium-containing nanoparticles, *Aerosol Science and Technology*, 52(9), 971-983, https://doi.org/10.1080/02786826.2018.1484071, 2018

1 Introduction

The average volume of inhaled air per minute by an adult is around 10 liters (EPA, 2011). Depending on both the location and time of the year, this volume of outdoor air contains from 10^5 to 10^{10} solid or liquid particles (Seinfeld and Pandis, 2016).

The solid and liquid particles and the air surrounding them form a colloid called the atmospheric aerosol. If one assumes a global average particle concentration of 1 μgm^{-3} , then the lowest part of the Earth's atmosphere, the troposphere, contains approximately 2 Tg of particles. These particles affect our life both positively and negatively through the weather and climate, and they may even cause a variety of diseases.

This thesis focuses on quantifying some of the important properties of organic aerosol particles; it is known that they affect the dynamics of atmospheric aerosols, but they are difficult to measure directly. In particular, this thesis concentrates on how these properties can be characterized by combining laboratory measurements and state-of-the-art numerical modelling.

The thesis consists of eight chapters, which summarize the research presented in five scientific articles. In the rest of this first chapter, a somewhat more in-depth introduction is provided to the world of atmospheric aerosols and to the role of organic compounds in these particles. In the first chapter, the aims of the thesis are also defined. Chapter 2 presents the properties of organic compounds and particles that were studied. Chapter 3 describes the numerical models and methods used. Chapters 4 through 6 summarize the key results obtained in the thesis. The topics of each scientific article and my contribution in each of them are covered in chapter 7 and conclusions are presented in chapter 8. The scientific articles are included at the end of the thesis.

1.1 Atmospheric aerosols and their impacts

Atmospheric particles have different shapes and sizes although in computational models and calculations, the particles are usually assumed to have a spherical shape and consequently, diameter or radius is used as a characteristic length. Deviations from this shape can be handled by introducing a shape correction factor (Seinfeld and Pandis, 2016).

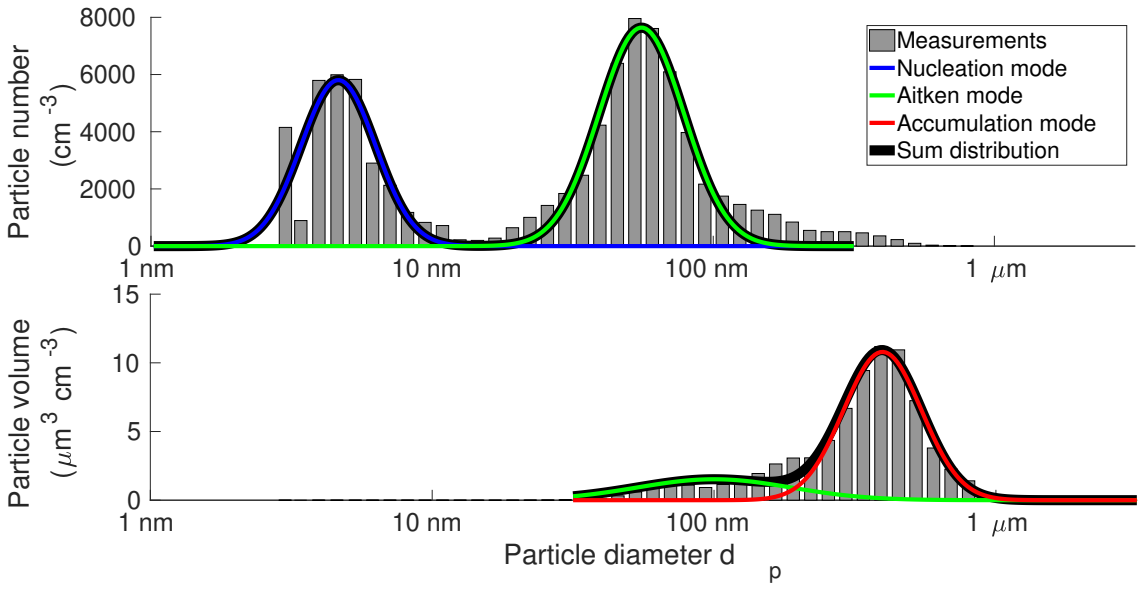

Figure 1.1: Particle number distribution (upper panel) and particle volume distribution (lower panel) from SMEAR IV station Puijo, Kuopio, Finland. Measurement data are from July 2nd, 2019 early in the morning. The figure also illustrates fitted multi modal distribution (black line) and the three log-normal distributions that make up the sum distribution (blue: nucleation mode, green: Aitken mode, red: accumulation mode)

Figure 1.1 shows an example of particle size distributions in both particle number and volume bases, from SMEAR IV station Kuopio, Finland gathered on July 2nd, 2019. Three distinct modes can be seen in the data. The first mode from the left is called the nucleation mode. This mode consists of particles with diameters of a few nanometers. The nucleation mode particles are formed from nucleation of sulfuric acid and bases such as amines and ammonia (Kulmala et al., 2000, 2004; Almeida et al., 2013) as well as oxidized organic compounds (Riccobono et al., 2014; Dunne et al., 2016). The second mode illustrated in Fig. 1.1 is called the Aitken mode. The particles in the Aitken mode originate from the growth of nucleation mode particles by organic and inorganic vapors, but also from the emission of particles released in various combustion processes e.g combustion of fuels (Seinfeld and Pandis, 2016). In both the nucleation and the Aitken mode, the particles are effectively scavenged by coagulation[1] into larger particles (Seinfeld and Pandis, 2016).

[1]collisions between particles where one particle sticks to another

The third mode is called the accumulation mode; it consists of particles with diameters from few tens of nanometers to a couple of micrometers. This mode is the most prevalent in the lower panel of Fig 1.1 since the size distribution is predominated by particles formed through coagulation and also from the growth of nucleation and Aitken mode particles. The particle removal mechanisms e.g. wet and dry deposition are also the least efficient in this region (Seinfeld and Pandis, 2016). One mode not shown in Fig 1.1 is the coarse mode which consists of particles with sizes larger than 2.5 μm. These particles originate from anthropogenic activities and natural sources like wind-blown dust or sea spray.

On a global scale, particles with a diameter smaller than 1 μm consist of both inorganic and organic compounds (Zhang et al., 2007). The inorganic fraction consists mostly of sulfate, nitrate and ammonium. The organic fraction contains a multitude of different compounds which are discussed more in sections 1.2 and 2.1. In addition to organic and inorganic compounds, atmospheric particles also contain water which is abundant in the atmosphere.

Atmospheric particles exert various effects on the climate and health. The two main quantities related to health effects of particles and air quality are PM_{10} and $PM_{2.5}$. PM_{10} refers to particulate matter whose size is smaller than 10 μm and $PM_{2.5}$ particulate matter whose size is smaller than 2.5 μm. It has been estimated that even an increase of 10 μgm^{-3} in $PM_{2.5}$ was responsible for increasing the mortality by over 1% on the following day in the USA (Franklin et al., 2007). However, the $PM_{2.5}$ and PM_{10} measures might not be capable of capturing all of the particles' health effects since the fraction of deposited particles greatly increase when particle size is below 100 nm (Löndahl et al., 2006)

Atmospheric aerosols impact both directly and indirectly on the climate. For example, the particles can either scatter solar radiation directly which has a cooling effect or absorb radiation which has a warming effect on the climate. These radiative effects depend on the chemical composition and size of the particles (Stocker et al., 2013; Yu et al., 2006).

The most poorly understood climate effect of atmospheric particles on the climate is their role on cloud formation and the subsequent properties of the formed clouds. In the Intergovernmental Panel for Climate Changes (IPCC) assessment report 5 (AR5) (Stocker et al., 2013) it was estimated that the indirect effect was cooling on average,

but our current knowledge is still far from complete about many important aerosol-cloud-interaction processes.

Atmospheric particles act as an initial liquid or solid phase on which supersaturated water vapor can condense, forming clouds (Seinfeld and Pandis, 2016). The amount of these cloud condensation nuclei depends most strongly on the particle size distribution with a secondary effect contributed by the composition of the particles (Dusek et al., 2006).

1.2 Organic compounds in atmospheric aerosols

Atmospheric particles can be emitted into the atmosphere directly, but they are also formed from the nucleation of sulfuric acid, bases and oxidized organic compounds (Kulmala et al., 2000; Riccobono et al., 2014). These two pathways are called the primary and secondary pathway, respectively. Particles formed from the secondary pathway have initially a size of a few nanometers and they need to grow substantially in order to have an effect on the climate. In many areas, the growth is due to condensation of low- and semi-volatile organic vapors onto the surface of the particles. (Riipinen et al., 2012, 2011; Kuang et al., 2010; Laaksonen et al., 2008; Kulmala et al., 2000). The organic compounds can condense also onto primary particles. The organic fraction of atmospheric particles contains thousands of different compounds (Goldstein and Galbally, 2007). Measurements of atmospheric particle composition are made with mass spectrometers. Instead of analyzing every compound individually, the compounds in a mass spectrometer data can be grouped into factors based on their chemical properties and sources and applying statistical dimension reduction techniques (SDRT) (e.g Zhang et al., 2011; Ulbrich et al., 2009; Zhang et al., 2005).

Zhang et al. (2007) reported a series of particle composition measurements from the Northern Hemisphere analyzed with a SDRT that allowed the organic fraction to be split into a hydrocarbon-like organic aerosol (HOA) and several types of oxygenated organic aerosol (OOA) types. The HOA factor is related to anthropogenic actions such as fossil fuel burning and primary emissions where particles enter the atmosphere directly (primary organic aerosol, POA). The OOA factors are linked to organic compounds produced from emissions and the subsequent oxidation of volatile organic compounds (VOCs). Organic particles formed from this secondary pathway are called a secondary

organic aerosol (SOA). A significant fraction of the total amount of organics in the particles originates from the OOA factors (Tsigaridis et al., 2014; Hallquist et al., 2009; Jimenez et al., 2009; Zhang et al., 2007).

The formation of SOA starts from the emission of VOCs which can be from both anthropogenic and biogenic origins; of these, biogenic sources clearly dominate the VOC budget (Goldstein and Galbally, 2007). These VOCs undergo rapid oxidation reactions with ozone (O_3) and hydroxyl radicals (OH) during the day and with ozone and nitrate radicals (NO_3) at night. The first oxidation reactions lead to organic radicals, which undergo further reactions in the atmosphere and form semi-volatile compounds (e.g. Glasius and Goldstein, 2016; Kroll and Seinfeld, 2008; Atkinson and Arey, 2003, and references therein). The semi-volatile compounds can partition into the available atmospheric particulate matter to form SOA or further oxidize either towards CO_2 or to compounds that have lower volatilities than the semi-volatile compounds. These low-volatility compounds partition to the particle phase more effectively than the semi-volatile compounds. The particle phase organic compounds undergo further reactions that alter their composition and properties (Kroll and Seinfeld, 2008) creating a complex mixture that exists in different phase states (Shiraiwa et al., 2017; Renbaum-Wolff et al., 2013; Koop et al., 2011; Virtanen et al., 2010).

1.3 Aims of the thesis

If one wished to understand the interactions between aerosols, clouds and the climate, a detailed knowledge about the properties of organic aerosols and especially SOA is needed (Hallquist et al., 2009). The volatility and the phase state of SOA particles are two of the most important properties (Glasius and Goldstein, 2016); another important property is the particles' hygroscopicity, i.e., their ability to take up water.

This thesis presents the recent development in characterizing these properties from laboratory measurements using process modelling techniques. The aims of the thesis are

1. To develop and test a process model optimization method for estimating the volatility distribution of organic compounds in the OA particles as well as the viscosity of the particles from isothermal OA evaporation experiments.

2. To compare how well the volatility distribution can be estimated from data on the changes in particle size and from mass spectrometer data during isothermal OA evaporation experiments.

3. To estimate the volatility distribution, viscosity and enthalpy of vaporization of α-pinene derived SOA.

4. To test how accurately the hygroscopicity of dimethylamine-containing particles is modelled even at very smallest particle sizes in a state-of-the art thermodynamic equilibrium model.

2 On the studied properties

2.1 Partitioning of organic compounds – volatility

The tendency of an organic compound to evaporate from the particle (solid or liquid) phase to the gas phase is called its volatility. The thermodynamic property related to volatility is called the saturation vapor pressure (p_{sat}), which is defined as the vapor pressure of a pure compound over a pure condensed (solid or liquid) phase at thermodynamic equilibrium. The thermodynamic equilibrium is defined as the point where the temperature and the pressure of every phase (gas – liquid or gas – solid for aerosols) are equal and where there is no net flow of molecules to either phase. The condensed phase will be assumed to be liquid from now on for simplicity.

The condensed phase of aerosol particles consists usually of a mixture of different compounds with varying amounts and interactions between the molecules. For particles with a diameter less than ca. 100 nm the curvature of the particles has also an effect on the vapor pressure near the surface of the particle. Under these conditions, the equilibrium vapor pressure of compound i ($p_{eq,i}$) over the particle surface at thermodynamic equilibrium can be calculated from $p_{sat,i}$ as (e.g. Seinfeld and Pandis, 2016)

$$p_{eq,i} = x_i \, \gamma_i \, \mathrm{Ke} \, p_{sat,i}, \tag{2.1}$$

where x_i is the mole fraction of compound i in the condensed phase, γ_i is the mole-fraction-based activity coefficient of i and Ke is called the Kelvin term. The activity coefficient γ_i depends on the interactions between compound i with itself and with all other compounds in the particle. Unless otherwise stated, in this thesis γ is assumed to be unity and the particle phase is therefore assumed to behave ideally, i.e., the interactions of a compound i with itself are assumed to be equal to the interactions of i with other compounds. A non-ideal liquid particle phase is discussed in section 3.3 and studied in **Paper V**

The Kelvin term takes into account the curvature of the particle. The Kelvin term is defined as (Seinfeld and Pandis, 2016)

$$\mathrm{Ke} = \exp\left(\frac{4\sigma\nu_{m,i}}{RTd_p}\right), \tag{2.2}$$

where σ is the surface tension of the particle, $\nu_{m,i}$ is the molecular volume of compound i, R is the universal gas constant and d_p is the diameter of the particle. The terms inside the exponential in Eq. (2.2) are always positive and the Kelvin term is thus always larger than one. The curvature of the particle therefore increases the equilibrium vapor pressure.

The temperature effect to $p_{eq,i}$ can be taken into account by using the Clausius-Clapeyron equation for the saturation vapor pressure (e.g. Bilde et al., 2015)

$$p_{sat,i}(T) = p_{sat,i}(T_{ref}) \exp\left[\frac{\Delta H_{vap,i}}{R}\left(\frac{1}{T_{ref}} - \frac{1}{T}\right)\right], \tag{2.3}$$

where T_{ref} is a reference temperature and $\Delta H_{vap,i}$ is the specific enthalpy of vaporization, i.e., the heat required to evaporate one mole of compound i from the liquid phase to the gas phase. In the derivation of Eq. (2.3) the enthalpy of vaporization is assumed to be independent of the temperature.

Instead of vapor pressures, saturation and equilibrium mass concentrations (C_{sat} and C_{eq}) are more commonly used when dealing with atmospheric organic compounds. The concentration and pressure are related by an equation of state. Usually the gas phase is assumed to obey the ideal gas law, leading to $C = \frac{pM}{RT}$, where M is the molar mass. C_{sat} and C_{eq} are usually expressed in units $\mu\mathrm{gm}^{-3}$.

In theory, the volatility of organic compounds could be resolved by defining C_{sat} for every compound. In practice, this is not currently possible due to the vast number of different organic compounds in the atmosphere that can partition into the particles (Glasius and Goldstein, 2016; Goldstein and Galbally, 2007) and due to the significant uncertainties that are related to saturation vapor pressure measurements of even simple organic compounds, such as carboxylic acids (Bilde et al., 2015). Even if these challenges could be overcome, the results might be challenging to incorporate into global climate models because representing thousands of different organic compounds would require a huge amount of computational resources. Therefore, parametrizations have to be used.

Perhaps the most widely used volatility parametrization is the volatility basis set (VBS) proposed by Donahue et al. (2006). In a VBS, the organic compounds are grouped based on their C_{sat} or C^*. The C^* is called the effective saturation mass concentration and is defined as the product of the C_{sat} and activity coefficient γ of a compound

(Seinfeld and Pandis, 2016). The different volatility groups in the VBS are separated commonly by a single magnitude difference in C_{sat}. For example compounds with $\log(C_{sat}) = [0.5; 1.5[$ are grouped to bin $\log(C_{sat}) = 1$. An example of a VBS is shown in Fig. 2.1 where forty different compounds with different C_{sat} and particle phase mole fractions are grouped into six volatility bins. In this example, all the compounds with $\log(C_{sat}) \leq -3$ are grouped to the volatility bin $\log(C_{sat}) = -3$ and all the compounds with $\log(C_{sat}) \geq 2$ to volatility bin $\log(C_{sat}) = 2$. The volatility distributions presented in this thesis do not always group the compounds to bins with a decadal difference in C_{sat} between two adjacent bins as was done in the original work of Donahue et al. (2006), and therefore the term volatility distribution (VD) is used. The term VD compound is used to distinguish between organic and model compounds (volatility bins).

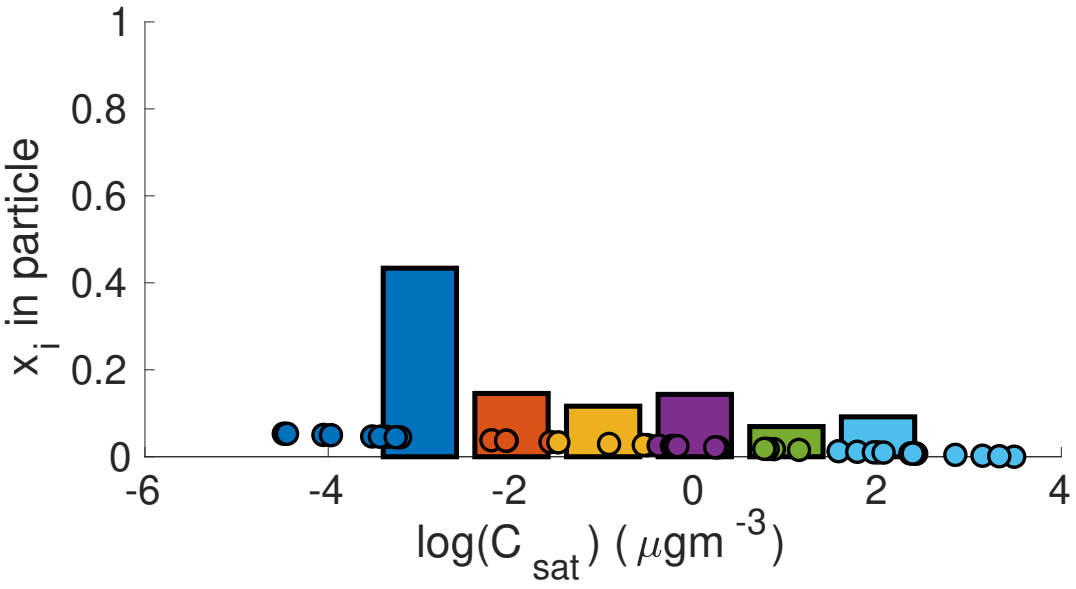

Figure 2.1: Example of forty organic compounds (circles) grouped to six volatility bins (bars). Each new bin to the right increases the C_{sat} by one order of magnitude. The color of a circle indicates to which volatility group the organic compound is assigned. The vertical axis shows the mole fraction in the particle phase. The data is from the artificial data set 4 in **Paper I**.

2.2 Amorphous phase of the particles – viscosity

Substances can be classified with the (dynamic) viscosity η into liquids ($\eta \leq 10^2$ Pa s), semi-solids ($\eta \approx 10^2 \ldots 10^{12}$ Pa s) and solids ($\eta \geq 10^{12}$ Pa s) (Koop et al., 2011; Shiraiwa et al., 2011). A higher viscosity refers to a slower movement of molecules along possible concentration gradients in matter and can be thought to represent the stiffness of the matter. The viscosity of commonplace substances can span more than several orders of magnitude. For example, a glass can have a viscosity $\eta_{glass} > 10^{12}$ Pa s whereas water at room temperature has $\eta_{water} = 10^{-3}$ Pa s (Rumble et al., 2018).

Virtanen et al. (2010) were the first to report laboratory measurements of an amorphous (semi-)solid state of SOA particles that had been hypothesized earlier by Zobrist et al. (2008). The amorphous phase refers to a physical state of matter where the matter does not exhibit a long-range order (Meille et al., 2011) i.e. unlike the situation in crystals. Until the work of Virtanen et al. (2010) model representations of organic aerosols assumed that the particle phase behaved like a liquid. After the report of Virtanen et al. (2010), SOA related research has concentrated on the quantification of the viscosity of SOA (e.g. Rovelli et al., 2019; DeRieux et al., 2018; Reid et al., 2018; Song et al., 2016; Järvinen et al., 2016; Renbaum-Wolff et al., 2013; Abramson et al., 2013). The viscosity of SOA particles is important because it determines whether the particle dynamics are controlled solely by the volatility of individual compounds or whether the movement of the compounds inside the particles also plays a role (Shiraiwa et al., 2011). Examples of how viscosity affects the evaporation of organic compounds from particles in laboratory experiments are seen in **Papers I–IV**

In the work presented in this thesis, the viscosity of the particles is assumed to have the form

$$\log \eta = \sum_{i=1}^{N} x_i \log b_i, \tag{2.4}$$

where b_i is the contribution parameter of compound i to the viscosity of the particle and the sum goes from 1 to the number of compounds N in the particle. In an ideal case, the contribution parameter b_i can be thought to represent the viscosity of the pure substance similarly to what O'Meara et al. (2016) used for the self-diffusion coefficients of viscous aerosol particles. In this thesis Eq. (2.4) was used to calculate the viscosity

of particles in **Papers I–IV** using VD compounds in place of real compounds.

2.3 Water uptake of particles – hygroscopicity

The interaction of water with inorganic and organic compounds is important because water is the most abundant vapor in the atmosphere (Seinfeld and Pandis, 2016). The tendency of aerosol particles to absorb moisture from the atmosphere is called hygroscopicity. If ideal partitioning of water to particle phase were to be assumed, at thermodynamic equilibrium the amount of water in the particle could be calculated from solving x_{water} from Eq. (2.1) assuming $\gamma_{water} = 1$

$$\begin{aligned} x_w &= \frac{p_i}{p_{sat}\mathrm{Ke}} \\ &= \frac{S}{\mathrm{Ke}}, \end{aligned} \tag{2.5}$$

where S is the saturation ratio (relative humidty (RH) divided by hundred) of water and the subscript w refers to water. However, water molecules are polar meaning the interaction of water with itself and with other compounds are not equal. The ideal solution assumptions in Eq. (2.5) is therefore not adequate. Including γ_w into Eq. (2.5) results in

$$\begin{aligned} \gamma_w x_w &= \frac{S}{\mathrm{Ke}} \\ a_w &= \frac{S}{\mathrm{Ke}}, \end{aligned} \tag{2.6}$$

where a_w is called the activity of water.

In practice, if there are multiple compounds in the studied system, γ_w depends on the relative amounts of all of the compounds (e.g. Clegg et al., 2001). If one wishes to calculate the amount of water in a particle at thermodynamic equilibrium, the amounts of all the compounds and their activity coefficients need to be known. As the number of compounds increases the calculation soon becomes too difficult to calculate explicitly. For this reason, there exists multiple numerical models that calculate the

composition of a system at thermodynamic equilibrium e.g. E-AIM (Wexler and Clegg, 2002) AIOMFAC (Zuend et al., 2008, 2010) and uManSysProp (Topping et al., 2016). The first of the models is presented shortly in section 3.3 and its capability to evaluate water uptake of dimethylamine containing particles was determined in **Paper V**.

3 Process modelling and model optimization

The principal work done in this thesis concentrates on modelling aerosol processes and estimating the properties of organic aerosols from such modelling efforts. In **Papers I** through **IV**, the evaporation of organic compounds from particles has been modelled in both low and high particle phase water content cases. When the particle phase water content is high, the viscosity of the particles is lower. In **Paper V**, the water uptake of dimethylamine-containing organic-inorganic particles was modelled. In this section all the process models used in this thesis and their mathematical background are presented. Additionally, a global optimization algorithm is presented for identifying a model input that produces the desired model output.

3.1 Evaporation from a liquid-like phase

If the particle surface is in thermodynamic equilibrium with the gas phase directly above the surface, the evaporation (or condensation) of a compound i is driven by the difference between the gas phase concentration far from the particle C_i and the equilibrium vapor concentration $C_{eq,i}$. The mass flux (change in mass of compound i in time) $I_{m,i}$ can be stated as (Seinfeld and Pandis, 2016; Lehtinen and Kulmala, 2003; Vesala et al., 1997)

$$I_{m,i} = 2\pi(d_p + d_i)(D_{g,p} + D_{g,i})\beta_{m,i}(C_i - C_{eq,i}), \tag{3.1}$$

where d_i is the diameter of molecule, $D_{g,p}$ is the diffusion coefficient of the particle in a gas, $D_{g,i}$ is the gas phase diffusion coefficient of molecule i and $\beta_{m,i}$ is the mass flux correction factor.

The distance that the gas molecules travel between two collisions is called the mean free path of a gas. The derivation of Eq. (3.1) starts from assuming that the mean

free path of the gas molecules is small when compared to the size of the particle. In this case the gas phase is a continuum from the point-of-view of the particle. The $\beta_{m,i}$ corrects the (continuum regime) mass flux such that Eq. (3.1) can be used also when the particle size is smaller or comparable to the distance gas molecules travel between collisions with each other. There are multiple derived correction factors (Seinfeld and Pandis, 2016). In this thesis the Fuchs-Sutugin form of the mass flux correction factor was used (Fuchs and Sutugin, 1971)

$$\beta_{m,i} = \frac{1 + \mathrm{Kn}_i}{1 + \left(\frac{4}{3\alpha_{m,i}} + 0.377\right)\mathrm{Kn}_i + \frac{4}{3\alpha_{m,i}}\mathrm{Kn}_i^2}, \tag{3.2}$$

where $\alpha_{m,i}$ is the mass accommodation coefficient and Kn_i is the Knudsen number of compound i. The mass accommodation coefficient describes the probability that an organic compound will condense upon collision with the particle. In general, the mass accommodation coefficient of organic compounds has been found to be near unity (Julin et al., 2014) and consequently the mass accommodation coefficients are assigned the value $\alpha_{m,i} = 1$ for all compounds in this thesis.

In Eq. (3.2) the Knudsen number Kn_i is the ratio between the mean free path of the gas molecules λ_i and the particle size.

$$Kn_i = \frac{2\lambda_i}{d_p + d_i}. \tag{3.3}$$

The mean free path of a molecule in the gas phase when using Eq. (3.1) is calculated as

$$\lambda_i = \frac{(D_{g,p} + D_{g,i})}{(\bar{c_p}^2 + \bar{c_i}^2)^{1/2}}, \tag{3.4}$$

where $\bar{c_p}$ and $\bar{c_i}$ are the mean speeds of the particle and molecule i in the gas phase. If the speeds of a molecule and particle are assumed to be distributed according to the Maxwell-Boltzmann distribution, the mean speed can be calculated as the expected value of this distribution resulting in

$$\bar{c} = \sqrt{\frac{8kT}{\pi m}}, \tag{3.5}$$

where m is either the mass of a particle or of a molecule i.

In **Papers I–IV**, the evaporation of organic molecules from the liquid phase is calculated by solving simultaneously Eq. (3.1) for all the organic compounds and calculating the total particle mass flux as

$$\frac{dm_p}{dt} = \sum_{i=1}^{N} I_{m,i}, \tag{3.6}$$

where m_p is the mass of the particle and the sum goes from 1 to the number of organic (or VD) compounds in the particle.

The MATLAB program that solves these equations numerically is called the liquid-like evaporation model (LLEVAP). Figure 3.1 shows a schematic representation of the modelled system in the LLEVAP model. Eq. (3.1) are solved only for the organic compounds. When Eq. (3.1) are solved from a specified start time to an end time, the particle phase water fraction is constantly updated to keep the gas–particle equilibrium for water, assuming an ideal solution (Eq. 2.5).

As an output the LLEVAP model calculates the particle diameter d_p relative to the input starting diameter d_{p0} as a function of time by converting the particle mass from Eq. (3.6) to particle diameter. The resulting quantity is called the evaporation factor ($EF(t) = \frac{d_p(t)}{d_{p,0}}$).

In **Paper I**, Eq. (3.1) is used to model evaporation in an experimental setup where the gas phase is continuously flushed with a flow of nitrogen gas (N_2). This has an effect on Eq. (3.1) because the flow transfers molecules away from the near gas phase. This can be done by multiplying the mass flux $I_{m,i}$ with the Sherwood number Sh (e.g. Seinfeld and Pandis, 2016)

$$\mathrm{Sh} = \mathrm{Sh}_0 + \mathrm{Sh}_1 Re^{1/2} Sc^{1/3}, \tag{3.7}$$

where Re is the Reynolds number and Sc is the Schmidt number

$$Re = \frac{\rho_{g,N_2} v_{N_2} d_p}{\eta_{g,N_2}} \tag{3.8}$$

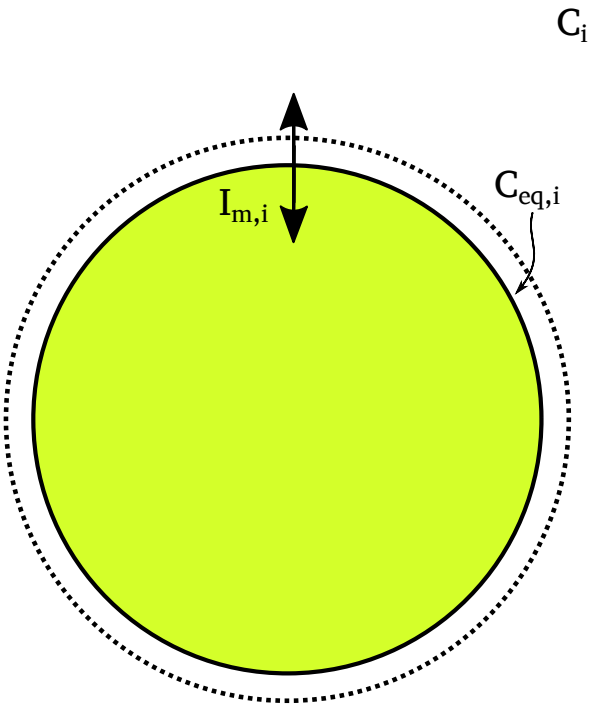

Figure 3.1: Schematic representation of the modelled system in the LLEVAP model. The mass fluxes $I_{m,i}$ are solved only for the organic compounds whereas the amount of water in the particle is constantly updated to ensure that there is an equilibrium between gas and liquid phase. The gas and particle phases are assumed to equilibrate instantly in the dashed region such that the evaporation is controlled by the equilibrium concentration $C_{eq,i}$ on the surface of the particle and gas phase concentration C_i far away from the particle given by Eq. (3.1).

$$Sc = \frac{\eta_{g,N_2}}{\rho_{g,N_2} D_{N_2}}, \tag{3.9}$$

where ρ_g is the density and η_g is the viscosity in the gas phase. v is the speed of the flow. In **Paper I** the constant terms Sh_0 and Sh_1 were set to $Sh_0 = 2.009$ and $Sh_1 = 0.514$ (Kulmala et al., 1995).

3.2 Diffusion inside the particles

The diffusion of organic molecules in a condensed phase can be modelled with Fick's first law of diffusion which states that the flux of compound i per unit area is proportional to the concentration gradient of the compound (e.g. Seinfeld and Pandis, 2016)

$$\begin{aligned} J_i &= D_{c,i} \nabla C_{c,i} \\ &= D_{c,i} \frac{\partial C_{c,i}}{\partial r}, \end{aligned} \tag{3.10}$$

where D is the diffusion coefficient of i and $C_{c,i}$ is the number concentration of i in the condensed phase. The last line of Eq. (3.10) follows when spherical symmetry is assumed.

The diffusion coefficient can be calculated from the viscosity of the condensed phase using the Stokes-Einstein equation and assuming spherical shape for the molecules (Einstein, 1905)

$$D_{c,i} = \frac{k_B T}{6 \pi r_i \eta}, \tag{3.11}$$

where k_B is the Boltzmann constant and r_i is the diameter of the molecule.

The Stokes-Einstein equation (3.11) is only valid for solutions where the collisions between molecules can be said to be random (i.e., in an ideal solution), where the viscosity is below that of a glass (10^{12} Pa s) and where the size of other molecules are much smaller than that of molecule i (e.g. Price et al., 2015; Miller, 1924).

While the first and second restrictions might be fulfilled for organic compounds in the particle phase, the third restriction most surely is not, as the organic molecules have comparable sizes. Furthermore, the Stokes-Einstein equation is also used in this thesis to calculate the diffusion coefficient of water, which is a much smaller molecule than the other organic molecules in the particle. The water diffusion coefficients in secondary organic material calculated with the Stokes-Einstein equation are many orders of magnitude smaller than the measured ones (Price et al., 2015). Whether the

Stokes-Einstein equation holds or not for the OA studied in this thesis has an effect to the reported viscosity values, but not on the calculation of diffusion inside the particle, which are performed using the diffusion coefficient $D_{c,i}$.

To model the particle evaporation in conditions, where the viscosity of particles is suspected to affect the particle dynamics, the kinetic multi-layer model of gas–particle interactions in aerosols and clouds (KM-GAP) developed by Shiraiwa et al. (2012) was used. In KM-GAP, the particle is divided into L co-centric layers and the flux of molecules i in layer l is calculated with Eq. (3.10) (Shiraiwa et al., 2012)

$$\begin{aligned}
\frac{dN_{i,l}}{dt} &= J_i A_l + J_i A_{l-1} \\
&= (J_{i,l,d} - J_{i,l,u}) A_l + (J_{i,l+1,u} - J_{i,l+1,d}) A_{l+1} \\
&= D_{c,i,l} \frac{\Delta C_{c,i,l,l-1}}{\Delta r_{l,l-1}} A_l + D_{c,i,l+1} \frac{\Delta C_{c,i,l,l+1}}{\Delta r_{l,l+1}} A_{l+1} \\
&= \frac{2D_{c,i,l}}{\delta(l) + \delta(l-1)} \left(C_{c,i,l-1} - C_{c,i,l}\right) A_l + \frac{2D_{c,i,l+1}}{\delta(l) + \delta(l+1)} \left(C_{c,i,l} - C_{c,i,l+1}\right) A_{l+1},
\end{aligned} \tag{3.12}$$

where A_l is the surface area of layer l and r_l is the length from the center of the particle to the layer l. Subscript $l-1$ refers to the layer above layer l and $l+1$ to the layer below l. The second line in Eq. (3.12) divides the molecular fluxes into fluxes that go through layer l (the first term) and those that go through the layer below l. The average distance that the molecules i travel when they move between two layers on the fourth row is expressed as

$$\Delta r_{l,l+1} = \frac{\delta(l) + \delta(l+1)}{2}, \tag{3.13}$$

where $\delta(l) = r_l - r_{l-1}$. A schematic representation of the molecular fluxes in the particle bulk is shown in Fig. 3.2.

When modelling the evaporation in **Paper III** the viscosity of the particles was calculated according to Eq. (2.4). In **Papers I–II** and **IV** the viscosity was calculated for each layer separately

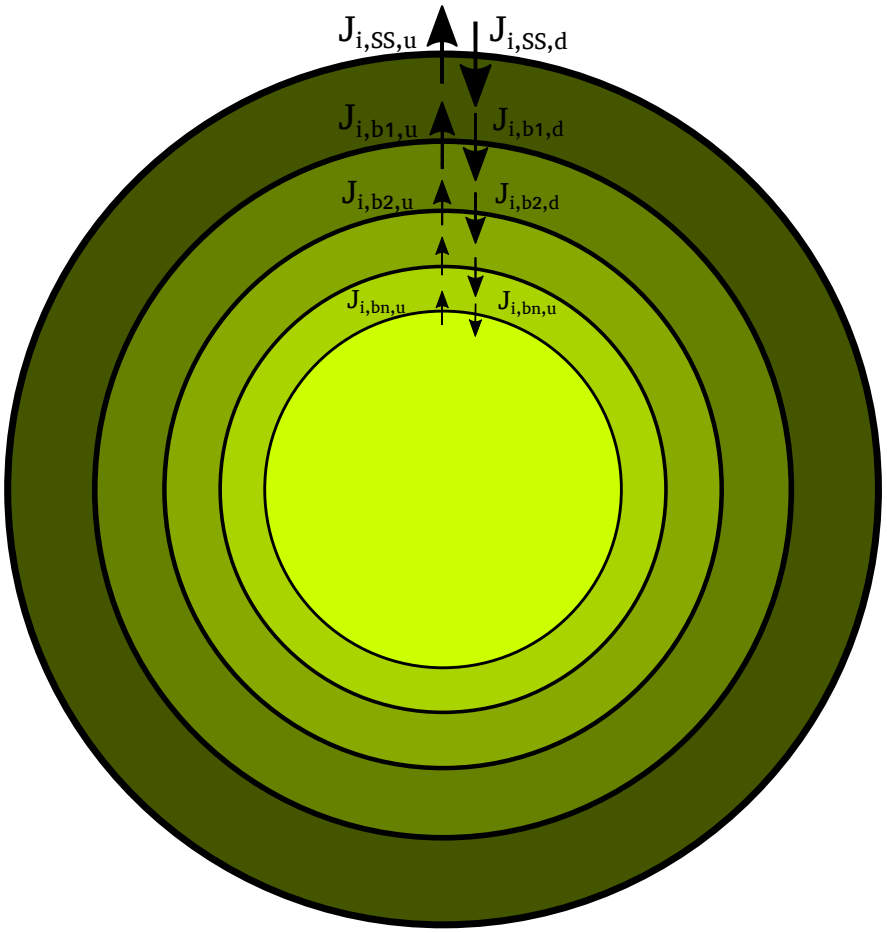

Figure 3.2: Representation of the modelled molecular diffusion in the KM-GAP model. In each bulk layer (b) and quasi-static surface layer (SS) the molecular flux of compound i to and from the layer is calculated according to Eq. (3.12). Different colors demonstrate that the composition differs between layers but only in the radial direction.

$$\log(\eta_l) = \sum_{i=1}^{N} x_{i,l} \log(b_i), \tag{3.14}$$

where $x_{i,l}$ is the mole fraction of i in layer l.

The first particle phase surface layer in KM-GAP is called the quasi-static surface (SS) layer. The SS-layer shrinks when evaporation is modelled as the compounds diffuse into the gas phase. To prevent negative concentrations, the SS-layer was combined with the first bulk layer if the size of the layer decreased below 0.3 nm in **Papers**

I–IV. The combination of layers during evaporation can result in unrealistic fluxes to the gas phase if the viscosity in the SS-layer is high and it is combined with a layer that has a considerably lower viscosity and contains high volatility compounds. To prevent such results the number of layers needs to be large enough. In general the number of layers in this thesis are between 30 and 60 and the final results were always checked by running the KM-GAP model with more than 100 layers.

3.3 Hygroscopicity of real solutions

In **Paper V**, the Extended Aerosol Inorganics Model's (E-AIM) (Wexler and Clegg, 2002; Clegg et al., 1998) capability to predict the hygroscopicity of dimethylamine, sulfate and ammonium containing nanoparticles at various RH levels and particle sizes was tested. E-AIM solves the equilibrium water content from the Gibbs free energy G of a system defined as (Wexler and Clegg, 2002)

$$\begin{aligned} G = {} & n_{c,w} RT(\ln a_w - \ln RH) \\ & + \sum_i n_i(\Delta_f G_i^0 + RT \ln a_i) \\ & + n_{g,w}(\Delta_f G_w^0 + RT \ln p_w), \end{aligned} \tag{3.15}$$

where $n_{c,w}$ is the moles of water in the condensed phase, and $n_{g,w}$ is the number of moles of water in the gas phase. $\Delta_f G_i^0$ is the Gibbs free energy or formation, i.e., the change in Gibbs free energy when one mole of compound i is formed. The sum in the second line in Eq. (3.15) goes from one to the number of species in the condensed phase excluding water.

To find the amount of water in the condensed phase when only the RH and the amount of all other compounds are known, the minimum of the Gibbs free energy needs to be calculated. This can be done by solving the partial derivative of (3.15) with respect to $n_{c,w}$. In the E-AIM setup used in **Paper V**, the activity coefficients of ionic compounds were calculated based on the work of Clegg et al. (1992, 1998). For organic compounds, the activity coefficients were calculated using the UNIFAC model (Hansen et al., 1991; Fredenslund et al., 1975). For aqueous inorganic–organic mixtures, the activity coefficient of water in E-AIM was calculated as a sum of logarithms from water

interactions with itself, with inorganic compounds and with organic compounds (Clegg et al., 2001).

The E-AIM output represents the equilibrium amount of moles of water in the condensed phase. The growth factor GF of particles due to uptake of water was used to relate the moles of water to a measurable quantity.

$$\begin{aligned} GF(RH) &= \frac{d_{p,RH}}{d_{p,dry}} \\ &= \left(\frac{m_{p,RH}\rho_{p,dry}}{m_{p,dry}\rho_{p,RH}} \right)^{\frac{1}{3}}, \end{aligned} \tag{3.16}$$

where ρ is the condensed phase density and subscripts RH and dry refer to quantities at a distinct RH and in a dry condition, respectively. The condensed phase densities are needed to calculate the GF. In real solutions, the volume and the density of a mixture can not be calculated as a sum of the volumes of individual compounds. Because of the interactions between the compounds, the volume of a mixture will differ from the summed volumes. The E-AIM calculates the density of a real solution by taking into account these interactions (Clegg and Wexler, 2011). Finally, to calculate the equilibrium saturation ratio over curved surface using (2.6) one needs to determine the surface tension σ of the condensed phase. The surface tension model used in E-AIM is presented in Dutcher et al. (2010).

3.4 Global optimization

The process models described in this section provide an answer to the question *"Given an input what is the evolution of the (modelled) system?"*. To estimate physicochemical properties, the question that is often asked is *"Given the evolution of the system, what was the initial stage (input)?"* because the evolution of the system is usually measured. Process models that describe the processes happening during the measurements can be used in finding the initial stage of the system.

The mathematical problem of finding the correct input that produces the wanted evolution can be stated as finding an input $\mathbf{x}$ that minimizes a function $f(\mathbf{x})$

$$\arg\min_{\mathbf{x}} f(\mathbf{x}). \tag{3.17}$$

$f(\mathbf{x})$ is called the *cost function* which is a function that returns smaller values when the input $\mathbf{x}$ produces a model output that better resembles the measurements. For example, given the measurement results $\mathbf{Y}_{measured}$ and a process model output $\mathbf{Y}_{model}(\mathbf{x})$, a cost function could be their mean squared deviation

$$f(\mathbf{x}) = \frac{1}{N}\sum_{i}^{N}\left(Y_{measuserd,i} - Y_{model,i}(\mathbf{x})\right)^2, \tag{3.18}$$

where the sum goes from one to the number of measurement results.

To find an input $\mathbf{x}_i$ such that there does not exists $\mathbf{x}_j$ for which $f(\mathbf{x}_j) < f(\mathbf{x}_i)$, the partial derivatives of f with respect to input $\mathbf{x}$ need to be calculated. In this case, $f(\mathbf{x_i})$ is the global minimum of f and $\mathbf{x_i}$ is the answer to the optimization problem presented in (3.17). The derivatives can be calculated in simple cases by hand. With more difficult cases, a numerical approximation can be used. When $\mathbf{Y}_{model}$ is calculated using a process model, it might be challenging to evaluate exactly the partial derivatives, and on the other hand, the numerical approximation of the derivatives might not be accurate enough to guarantee convergence.

When it is challenging to evualte the partial derivatives of the cost function, it might be sufficient to search for a solution for $\mathbf{x}$ that results in a small value of the cost function even though it is not possible to be certain that the found solution is a global minimum. These sufficient solutions can be calculated using metaheuristic, derivative-free algorithms.

There exists various metaheuristic algorithms which are intended to find a sufficiently good and efficient solution to this kind of optimization problem (3.17). Many of these algorithms have been inspired by natural processes. For example, the particle swarm optimization algorithm (Eberhart and Kennedy, 1995) is inspired by the behavior of bird flocks and fish schools and the cuckoo search (Yang and Deb, 2009) mimics the nesting behavior of certain species of cuckoos. The genetic algorithm used in this work (e.g. Goldberg, 1989) resembles natural evolution.

3.4.1 Monte Carlo genetic algorithm (MCGA)

The Monte Carlo genetic algorithm (MCGA) (Berkemeier et al., 2017, **Paper I**) is a metaheuristic optimization algorithm. MCGA is a hybrid algorithm, i.e., the algorithm combines two different optimization algorithms, a random search of the parameter space (Monte Carlo or MC part) followed by a genetic algorithm (GA part) which utilizes the solutions found in the MC part as the input. Figure 3.3 shows the flowchart of the algorithm used in this work. The implementation of the algorithm in **Papers I, II** and **IV** is described below. In **Paper III**, a version of the genetic algorithm was used and its differences to the GA part are also described.

In the MC part, a predetermined number $N_{\text{pop,MC}}$ of candidate solutions $\mathbf{x}$ to the optimization problem are drawn randomly. From these candidates, $N_{\text{pop,GA}} \leq N_{\text{pop,MC}}$ solutions are chosen. First, N_{elite} candidates are chosen that result in the smallest values of the cost function f and then the rest of the candidates are chosen randomly. The chosen candidates form the first iteration of the genetic algorithm, called a generation. The group of candidates in the current generation is also referred to as the population.

The genetic algorithm calculates new generations, which results in a slow homogenization of the cost function values of the candidates. The N_{elite} candidates from the previous generation are automatically moved to the next generation. New candidates are calculated to fill the population in the next generation. A new candidate is calculated by first picking two candidates, performing a crossover to these candidates, implementing a mutation and then calculating whether the new candidate is accepted or rejected.

The two candidates are picked based on the cost function values of the population. The candidates are selected such that the probability to be chosen is

$$\text{P(choose candidate } n) \propto f(\mathbf{x}_n)^{-1}, \tag{3.19}$$

where $\mathbf{x}_n$ is nth candidate's input to the process models. The right hand side of Eq. (3.19) can also be called the fitness F of the candidate, i.e., a higher fitness value corresponds to a smaller value of the cost function. In Fig. 3.3, the stopping criteria are expressed using the fitness value rather than the cost function. In **Paper III**, this probability was set to be the negative exponential of the cost function divided by a scaling parameter.

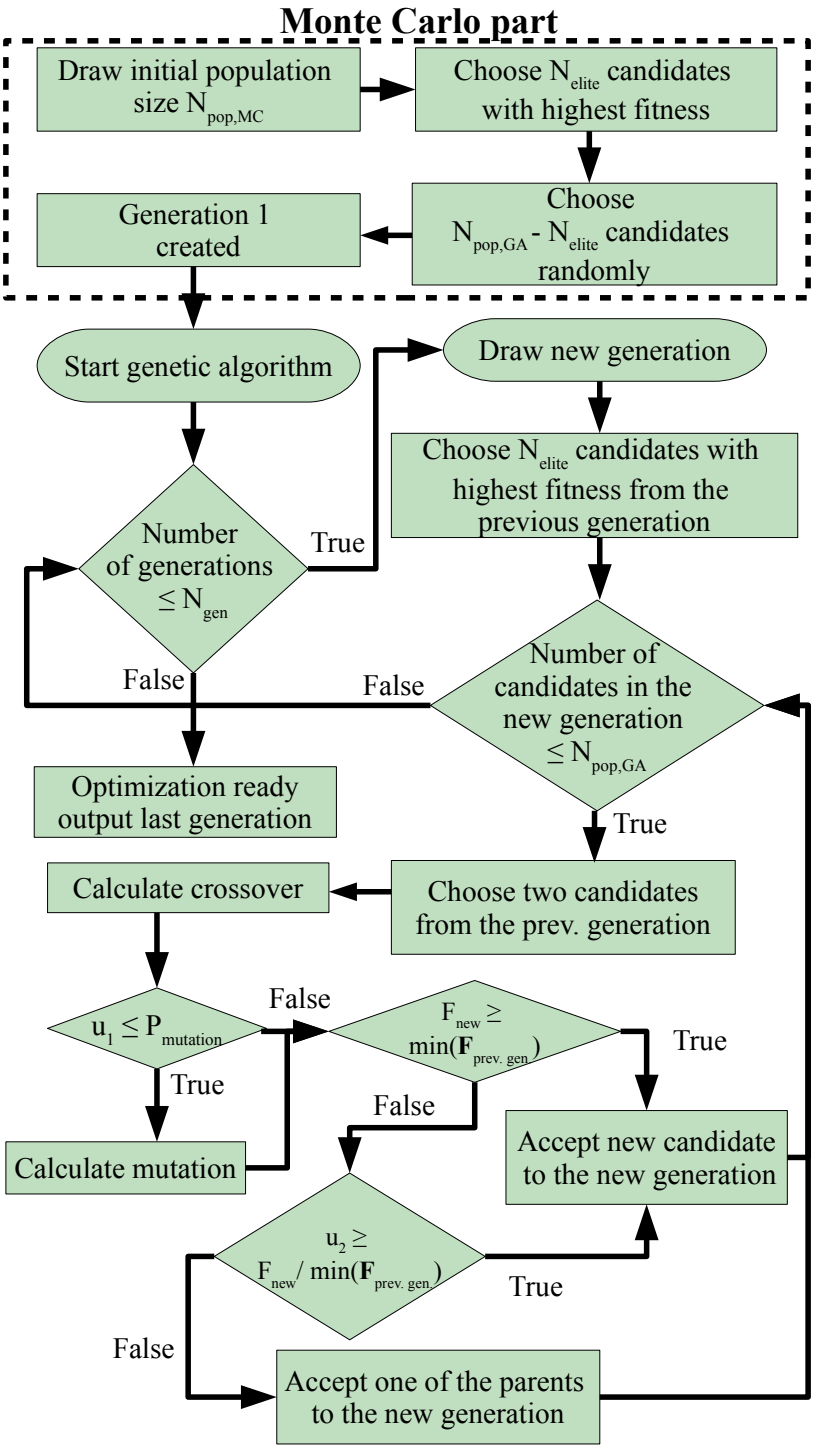

Figure 3.3: Flowchart of the MCGA optimization algorithm used in **Papers I, II** and **IV**. N_{pop} marks the number of candidates in either the MC or GA parts, N_{gen} the number of generations, N_{elite} is the number of highest fitness candidates that are always accepted to the new generation, F is the fitness of a candidate(s) (see text for definition). $\mathrm{F_{new}}$ refers to the fitness of a newly created candidate and $\mathbf{F}_{\text{prev. gen}}$ refers to all the fitness values in the previous generation. u marks a uniform random number in the range $]0, 1[$

The crossover is calculated by traversing a list of input variables from $\mathbf{x}$ that are marked as free or optimizable parameters[2]. For every free parameter, the MCGA algorithm picks either of the parent's parameter with equal probability. In **Paper III**, the crossover is calculated differently, taking into account both of the parent candidates' free parameter values (see the supplement of **Paper III**).

Once the candidate is created, it can undergo a mutation with a preset probability $\mathrm{P}_{\mathrm{mutation}}$. If the mutation happens, the free parameters are drawn again from their preset intervals.

Finally, the candidate is accepted to the new generation if its fitness is higher than the lowest fitness in the previous generation. If this is not the case, the candidate is accepted with a probability proportional to $\frac{F_{\mathrm{new}}}{min(F_{\mathrm{previous\ generation}})}$, where F_{new} is the fitness of the newly created candidate. If either of these conditions are not fulfilled, one of the parents is accepted to the next generation with a probability proportional to their fitness.

Figure 3.4 shows an example of how the cost function values of the population evolve during 10 generations of running the MCGA algorithm. The figure shows that the cost function values are distributed initially such that there are few good candidates and many more poor ones. As more generations are calculated the population homogenizes to candidates that have low cost function values.

In this thesis the MCGA algorithm was used to infer the volatility distributions at the start of the evaporation, enthalpies of vaporization and/or contribution parameter b_i values in Eq. (2.4). In a typical setup, the free parameters in the optimization were dry particle mole fraction of each VD compound at the start of the evaporation, the enthalpy of vaporization of each VD compound and the contribution parameter b_i values of each VD compound. The MCGA algorithm was set to search for those values of the free parameters that produce the measured evapograms when used as an input to either the LLEVAP or the KM-GAP model. The goodness-of-fit in all cases was calculated using Eq. (3.18).

[2]These variables are also called *design variables*

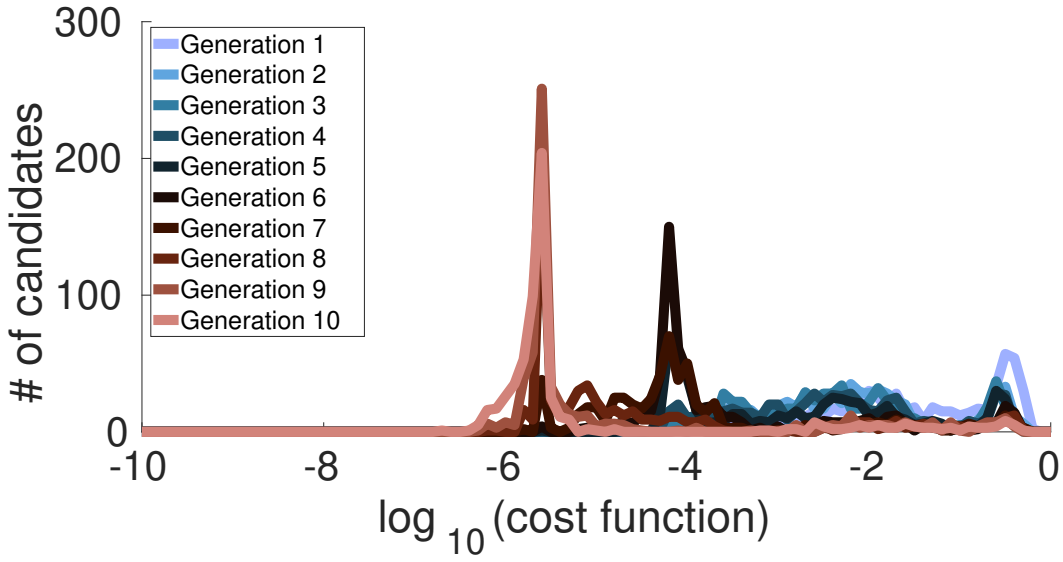

Figure 3.4: An example how the cost function values in a population evolve between generations. The horizontal axis shows the logarithm of the cost function (Eq. 3.18 and the vertical axis shows the number of candidates. Data is from **Paper I** where the MCGA algorithm was used to estimate volatility distribution of an artificial SOA particle

4 Methods to quantify volatility and viscosity from isothermal particle evaporation data

4.1 Isothermal evaporation measurements

There are several studies that have examined the kinetics and phase state of SOA by measuring the isothermal evaporation of the SOA particles (e.g., Grieshop et al., 2007; Vaden et al., 2011; Wilson et al., 2015; Liu et al., 2016; D'Ambro et al., 2018; Buchholz et al., 2019a, and **Papers I–IV**). The general experimental setup for isothermal evaporation studies in this thesis was

1. SOA formation
2. Evaporation condition selection
3. Sample selection
4. Gas phase dilution
5. Particle size measurement

In **Paper II**, the SOA was formed using the Potential Aerosol Mass (PAM) chamber (Kang et al., 2007; Lambe et al., 2011) and in **Papers III–IV**, a continuous flow tube reactor was used. The SOA generation requires a precursor VOC(s) (α-pinene in **Papers II–IV**) and oxidizing compound(s) (O_3 and/or OH in **Papers II-IV**). In all formation types, the VOCs are allowed to react with the oxidizing compounds to form an SOA. The oxidation conditions and the amount of VOCs have an influence to the resulting SOA.

In **Papers II-IV**, the SOA particles with diameter of 80 nm were selected with a differential mobility analyzer (TSI Inc., Model 3085) and led to a stainless steel reaction time chamber (RTC) where their evaporation was studied with a scanning mobility particle sizer (SMPS; TSI Inc., Model 3082+3775). When particles of a certain size were selected, the gaseous organic compounds were removed from the gas phase, which initiated the particle evaporation. The size distribution measurements in the RTC were started after its filling, which takes about 20 minutes. In order to obtain short residence time data, the selected monodisperse particles were led through a bypass

to the SMPS with tubing of varying sizes. The measurements result in particle size change versus time data which in this thesis is referred to as an *evapogram*.

An important aspect to keep in mind is that the conditions during the SOA formation (e.g. temperature and RH) were always similar in individual studies (**Papers I–IV**). When the SOA is formed under the same conditions, it has the same properties at the start of the evaporation even though the evaporation conditions might be different. For example, the volatility distributions are similar at the start of the evaporation even though the evaporation could be measured at two different RH levels.

Paper I tests the global optimization algorithm presented in Sect. 3.4.1 for estimating the VD and the viscosity. The aim was to test how well the algorithm, coupled with the presented process models, can estimate the properties of organic aerosol particles from isothermal particle evaporation experiments. In **Paper I**, the isothermal evaporation measurements were done with an electrodynamic balance (EDB) which traps an atomized droplet in an electric field and the size change is inferred by illuminating the droplet with a laser and measuring the elastically scattered light (Glantschnig and Chen, 1981; Davies et al., 2013; Rovelli et al., 2016; Marsh et al., 2017).

4.2 Volatility distribution estimated from isothermal evaporation data

The isothermal evaporation experimental setup in **Papers II–IV** constrain the volatility distribution (VD) compounds that can be estimated. First, the total gas phase concentration of organic compounds during SOA formation can not be higher than the total gas phase concentration near to the surface of the particles. This limits the maximum possible C_{sat} that can be estimated from the data, because the inequality

$$\sum_{i=1}^{N} x_i \,\mathrm{Ke}\, C_{sat,i} \leq C_{\mathrm{g,organics}}, \tag{4.1}$$

must hold. The gas phase concentration of organic compounds ($C_{\mathrm{g,organics}}$) can be calculated from the amount of reacted VOC precursor and the particle phase mass concentration that are both measured in **Papers II–IV**.

Second, the experimental time scale and particle size have an effect on the inferable VD. Any C_{sat} that is high enough to evaporate before the first measurement is not identifiable from the data and any C_{sat} that is low enough not to evaporate at all or only slightly during the experiment will be classified to the least volatile identifiable VD compound.

In **Papers I–II and IV**, the minimum and maximum C_{sat} that can be estimated from the measurements were determined by running the LLEVAP model with a particle that consists of one compound. The minimum identifiable C_{sat} was determined to be the value that showed at least 1% size change in the time scale of the experiments and the maximum to be the value that showed no more than a 90% size change before the first measurement point.

Figure 4.1 shows two examples from **Paper I**. Figure 4.1a shows MCGA estimates from optimizing the LLEVAP model output to match a synthetic data set. This data set is the same as shown in Fig. 2.1 and consists of 40 organic compounds, which differ only in their C_{sat}. These 40 compounds are grouped into six VD compounds whose mole fractions were optimized with the MCGA algorithm. The MCGA estimates are close to the correct values except for the two least volatile VD compounds. Both of these compounds evaporate more than 1% with respect to the experimental timescale, but at a such slow rate, there are many combinations of the two compounds that can produce the correct evapogram. The summed mole fraction of the two least volatile compounds is nearly constant between 500 independent estimates shown in **Paper I**.

Figure 4.1b shows the estimated VD of particles atomized from an aqueous mixture of sucrose (lower C^*) and glycerol (higher C^*). The evaporation of this mixture was measured with the EDB under two different RH condition. The LLEVAP and KM-GAP models were used to model the evaporation at high and low RH values, respectively. The estimated VD shows that the mole fraction of both compounds is captured well, but there is a slight deviation from the literature values when the volatilities are compared.

In **Paper I**, the difference in C^* estimate of glycerol was speculated to originate from the assumption that the particle phase behaves ideally in model simulations. AIOMFAC (Zuend et al., 2008, 2010) simulations using the initial particle composition revealed that the activity coefficient for water might be lower than unity, which means that amount of water to be underestimated in the LLEVAP and KM-GAP simulations where a water activity coefficient of one is assumed. In the optimization, this causes

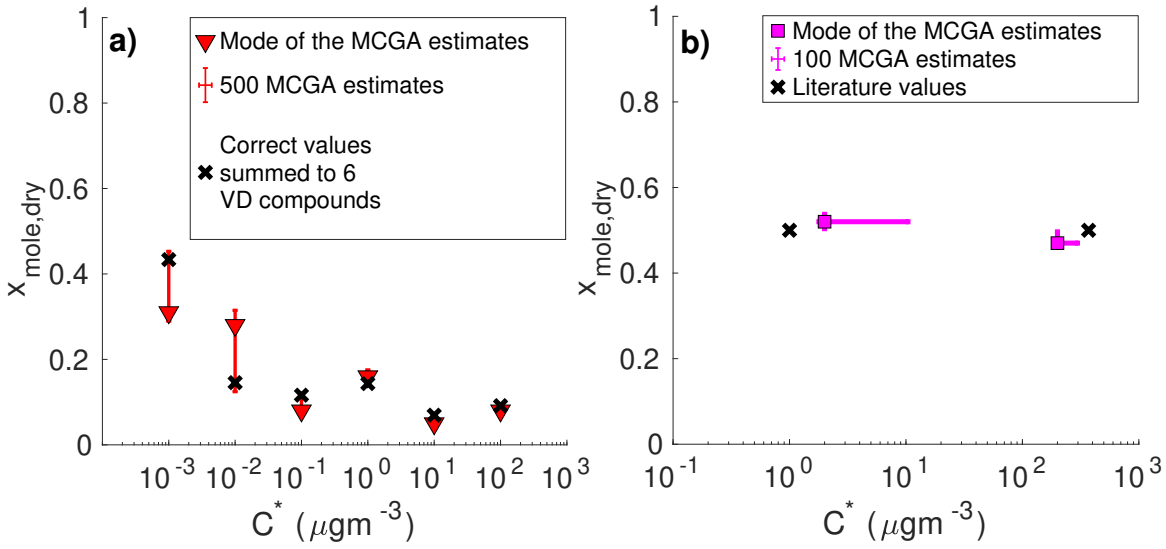

Figure 4.1: MCGA derived estimates for the volatility distribution of organic compounds in the particle phase at the start of the evaporation. The vertical axis shows the mole fraction in the particle excluding water and horizontal axis shows the effective saturation mass concentration C^*. a) artificial data set 4 in **Paper I** b) mixture 3 in **Paper I**.

the algorithm to underestimate the C^* of glycerol to obtain the correct evapogram.

4.3 Particle viscosity

The viscosity of SOA particles was also estimated in **Papers I–IV**. The experimental evapograms showed a consistently slower rate of evaporation in RH$\leq$20% conditions than in the high RH conditions, which is contrary to Eq. (3.1). At lower RH values the mole fraction of evaporating organics is higher and the evaporation rate should also be higher[3]. These results are in line with other evaporation studies at low RH (Vaden et al., 2011; Wilson et al., 2015) In **Papers I–IV**, these experimental results are interpreted such that the lower rate of evaporation at lower RH is due to mass transfer limitations in the particle phase, i.e., the particle phase viscosity is high enough to limit the diffusion of organics from the particle core to the surface where they evaporate into the gas phase.

[3]This result is also called the solution effect or Raoult's law

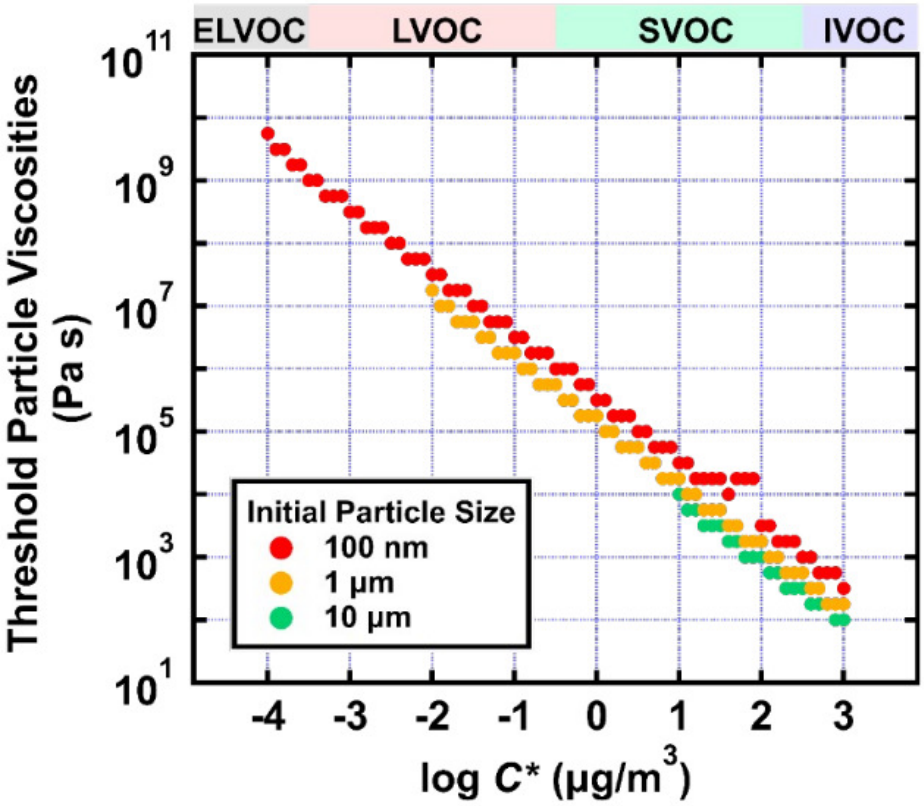

Figure 4.2: Threshold viscosity calculated in **Paper IV**. The threshold is determined to be that particle viscosity, where the LLEVAP and KM-GAP simulated evapograms differ by more than 1%. In the simulations the particle consisted of a non-volatile fraction and a volatile fraction whose C^* is shown in the horizontal axis. The initial particle size in these simulations was 80 nm. The top panel shows the volatility grouping typically used to describe the volatility of organic compounds (ELVOC: extremely low, LVOC: low-, SVOC: semi-, IVOC: intermediate volatile organic compound).

Figure 4.2 displays simulation results from **Paper IV** where the threshold viscosity for the studied evaporation process was calculated. The threshold viscosity was defined to be the particle phase viscosity, which limits the diffusion of organics to the surface such that the evaporation is not solely controlled by the VD of the organic compounds. This threshold value was calculated by simulating the evaporation of a particle that consists of non-volatile and volatile VD compounds. The horizontal axis in Fig. 4.2 shows the C^* of the volatile VD compound. The threshold viscosity was set to be the value where the KM-GAP simulated evaporation factors differed by more than 1% on average from the LLEVAP simulated evaporation factors.

Figure 4.2 shows that there exists a linear relationship with the $\log(C^*)$ of the evaporating VD compound and the threshold viscosity in the evaporation process. The particle size has an effect on the threshold viscosity. When the particle size is large, the threshold viscosity is lower than when the particle size is smaller.

Figure 4.2 shows also the minimum particle viscosity that is quantifiable from evaporation measurements in **Papers II–IV** since viscosities below the threshold limit are not sensitive to the evaporation process. In these low-viscosity fluids, the evaporation process is controlled solely by the volatility distribution. Similarly, when viscosity becomes high enough, virtually none of the organic compounds will evaporate during the experimental time scale. The viscosity thresholds depend on the particle size and VD of the organics in a complex way. For 80 nm particles and with typical VD obtained in this work, the quantifiable particle viscosity is around $\eta = 10^5$–10^{10} Pa s.

The mixing rule type of viscosity dependence on the mole fraction of the organic compounds (Eq. 2.4) in an ideal solution case makes it possible to quantify a pure compound's viscosity[4] η_0. In that case, the contribution parameter b_i is thought to be equal to η_0. The ability to infer η_0 from evaporation measurements with the process model optimization method was tested in **Paper I** with two simple mixtures consisting of water, sucrose and glycerol whose pure compound viscosities were known. Figure 4.3 shows that the estimated η_0 are far away from the literature values and that the estimated values are coupled to each other. The possible non-ideality of the studied solution could explain some of the discrepancy. The coupling of the free parameters presents clear challenges for estimating the viscosities of pure compounds from evaporation measurements with Eq. (2.4). There are too many options for the b_i values that produce the measured evapogram when used as an input to the KM-GAP model.

The fact that two pure compounds i.e. sucrose and glycerol, were not estimated correctly in **Paper I** does not mean that the overall particle viscosity could not be estimated correctly. The coupling of the b_i parameters as well as possible non-ideal behavior that affect the viscosity causes the b_i parameters to deviate from their literature values similar to that seen with the volatility of glycerol in Fig. 4.1b. On the other hand, the total particle viscosity is the quantity that is actually optimized when the optimization is performed against particle size change data. The total particle viscosity is correct if the system modelled with the KM-GAP model takes into account all the factors that affect the evaporation.

[4]viscosity of a solution that consists only of one compound

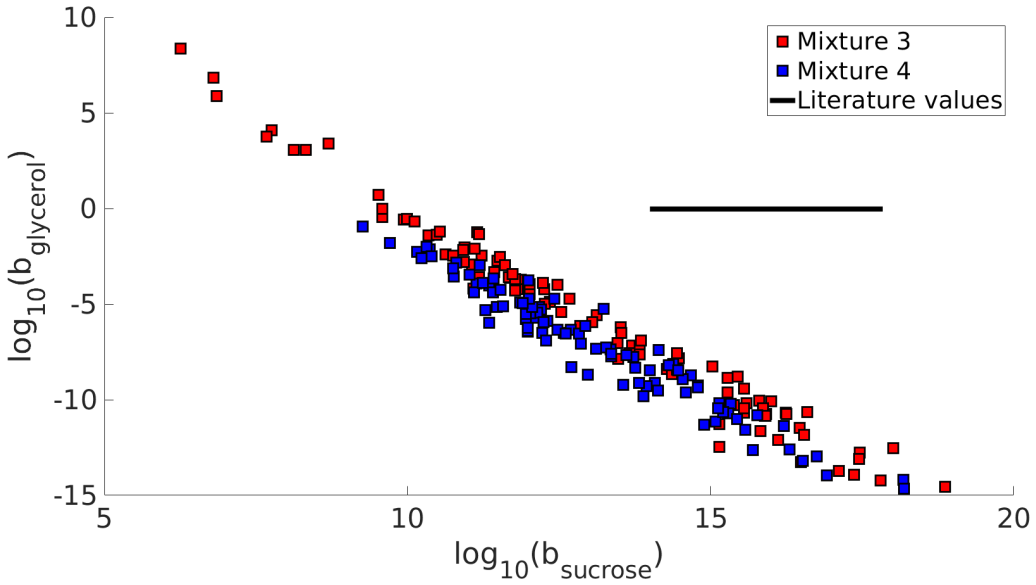

Figure 4.3: Pure compound viscosity for glycerol and sucrose estimated by optimizing process models to two different experimental data sets which differed in their particle water content during evaporation.

4.4 Volatility distribution estimated from mass spectrometer data

Paper II compares the volatility distributions estimated from particle size change measurements (see Sect. 4.2) and mass spectrometer measurements of the particles. The Filter Inlet for Gases and AEROsols (FIGAERO) (Lopez-Hilfiker et al., 2014) and Chemical Ionization Mass Spectrometer (CIMS) (Lee et al., 2014) were utilized to measure the particle phase composition during isothermal evaporation. The working principle of the FIGAERO inlet is that a particle sample is collected on a Teflon coated filter and heated with a flow of nitrogen gas. The applied heat volatilizes the organic compounds in the sample, which can be then detected in the CIMS.

The FIGAERO-CIMS measurement results in a matrix which shows how many counts the CIMS detected at a certain sample temperature and mass-to-charge ratio. In **Paper II**, this measurement matrix was analyzed using the positive matrix factorization (PMF) (Buchholz et al., 2019b; Paatero and Tapper, 1994) method to yield a volatility distribution. In order to distinguish between these two volatility distributions, the one inferred from evapograms is referred to as VD_{evap} and the one from PMF is referred to

as $\mathrm{VD_{PMF}}$.

PMF splits the measurement matrix $\mathbf{X}$ into three parts: mass loading profiles $\mathbf{G}$, mass spectra $\mathbf{F}$ and residual matrix $\mathbf{E}$ such that

$$\mathbf{X} = \mathbf{GF} + \mathbf{E}, \tag{4.2}$$

if the dimension of $\mathbf{X}$ is $m \times n$ then $\mathbf{G}$ is $m \times p$ matrix and $\mathbf{F}$ is $p \times n$ matrix where p is the number of PMF factors. The number of factors in the PMF analysis is a user defined parameter. An example of the mass loading profile $\mathbf{G}$ is shown in Fig. 4.4. In **Paper II**, the individual factors were interpreted to be VD compounds whose C^* can be calculated from the desorption temperature and the relative amount in the particle from the relative signal area in matrix $\mathbf{G}$

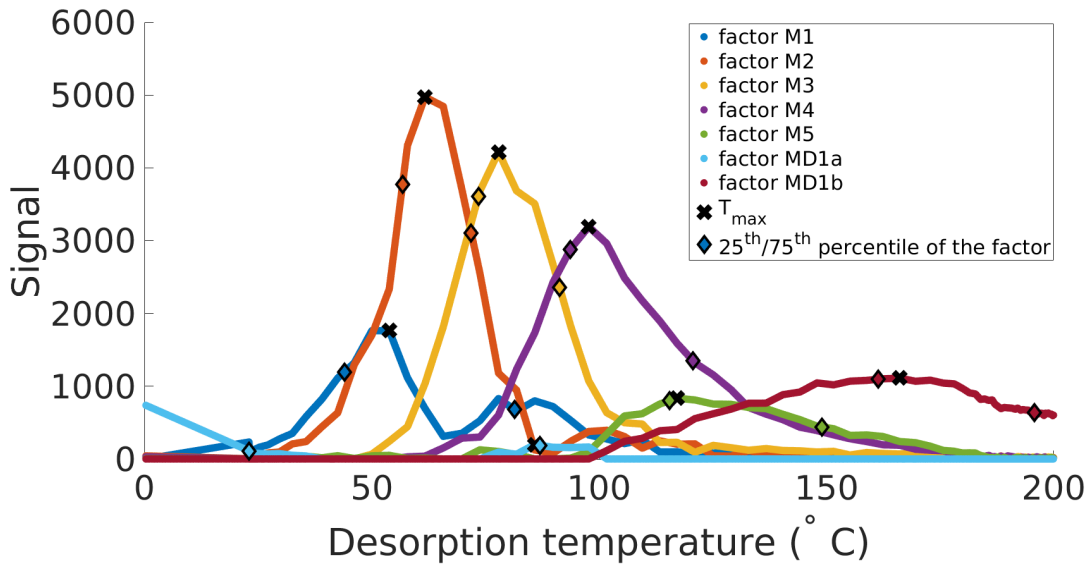

Figure 4.4: An example of the mass loading profile $\mathbf{G}$ in **Paper II**. The data is from a sample collected from medium O:C high RH evaporation measurement at the start of the evaporation.

Figure 4.5 shows the measured and simulated evapograms calculated using both volatility distributions as input to the LLEVAP model. In Fig. 4.5a the C^* in the $\mathrm{VD_{PMF}}$ are calculated using the maximum desorption temperature (black crosses in Fig. 4.4) and in Fig. 4.5b the C^* of $\mathrm{VD_{PMF,opt}}$ are calculated using the 25^{th} and 75^{th} percentiles

of each factors desorption temperature range (diamonds in Fig. 4.4). When these percentiles are converted to C^*, they form a range of possible values that the volatility of a factor can have. In Fig. 4.5b, the C^* of each factor was optimized with the MCGA algorithm to match the measured evapogram. The method shown in Fig. 4.5a does not produce a similar evapogram that which is measured while the method shown in Fig. 4.5b produces evapograms that match well with the measurements.

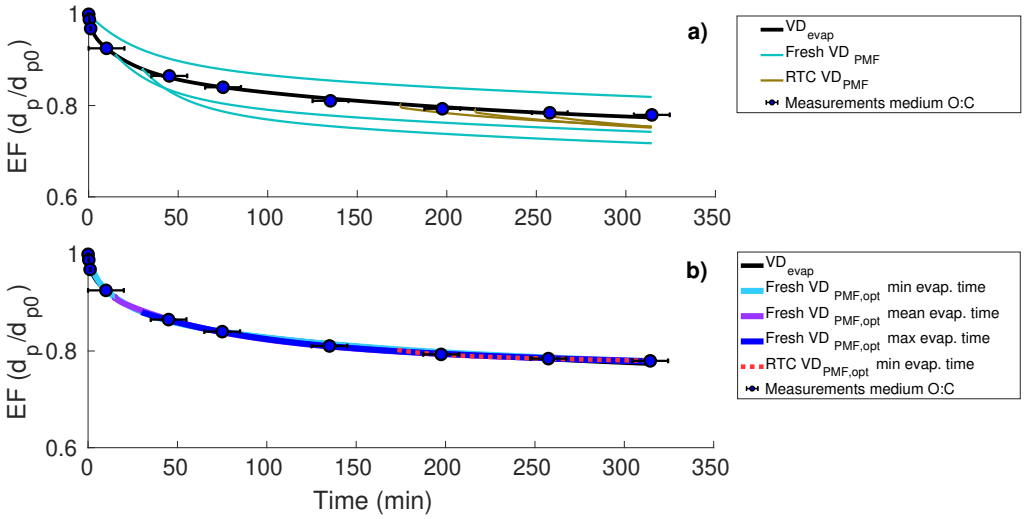

Figure 4.5: Measured and simulated evapograms of medium O:C high RH experiments in **Paper II**. The simulated evapograms are calculated using either $\mathrm{VD_{evap}}$ or $\mathrm{VD_{PMF}}$ as input. a) $\mathrm{VD_{PMF}}$, $\mathrm{C^*}$ are calculated using the maximum desorption temperature. There are three lines for both fresh and dry sample, which correspond to minimum, mean and maximum evaporation times seen also in subfigure b. b) $\mathrm{VD_{PMF,opt}}$, $\mathrm{C^*}$ are calculated using 25^{th}–75^{th} percentiles of the factors desorption temperature range. The minimum, mean and maximum evaporation time refer to times that the FIGAERO sample could have evaporated during sample collection.

The results of **Paper II** show that the two studied volatility distributions are comparable when each PMF factor's C^* is calculated from a range of desorption temperatures rather than from the maximum desorption temperature. Deriving the VD from mass spectrometer measurements would be an intriguing possibility for future parameter estimation studies from isothermal evaporation experiments as the mass spectrometer data constrains the parameter space beter than using only the particle size change measurements.

5 Volatility and viscosity of α-pinene SOA at different experimental conditions

Papers III–IV apply the process model optimization method described and tested in **Paper I** to analyze the properties of α-pinene SOA at various evaporation conditions. α-pinene is a cyclic monoterpene that is emitted from vegetation. Globally monoterpenes such as α-pinene comprise 16% of the total biogenic volatile organic compound annual yield and is one of the most important BVOCs in boreal forest regions (Guenther et al., 2012; Bäck et al., 2012).

The isothermal SOA evaporation measurements **Paper III** were performed at three different RH conditions (80%, 40% and ∼0%). The SOA was formed under dry conditions at room temperature with the exception of the first dry experiment where the RH was 30%. The SOA in **Paper III** was formed from ozonolysis of α-pinene. In **Paper IV**, the isothermal evaporation was measured at two different temperatures (10°C and 20°C) and at 4–5 different RH level. For the SOA produced from photo-oxidation of α-pinene, measurements were done at RH of 80%, 40%, 20% and ∼0% and for the SOA produced from ozonolysis of α-pinene the measurements were made at 80%, 40%, 30%, 20% and ∼0% RH. In **Paper IV**, the SOA was formed in RH between 33–36% and at room temperature.

As described in Sect. 4.1 the experimental evapograms show a suppressed evaporation rate for evaporation at dry conditions, contrary to what would be expected for liquid-like particles. In **Papers III–IV**, the process model optimization was done in two stages. First the evapogram(s) at highest RH (around RH≈ 80%) was taken and the dry particle mole fraction of each VD compound at the start of the evaporation was optimized to yield simulated evapogram matching to the measurements. Additionally, in **Paper IV** also the enthalpies of vaporization $\Delta H_{vap,i}$ of each VD compound were also optimized because the highest RH measurements were performed at two different temperatures. A linear relationship between $\Delta H_{vap,i}$ and $\log(C^*)$ was assumed, similarly to Epstein et al. (2009)

$$\Delta H_{vap,i} = k \log\left(C_i^*\right) + y, \tag{5.1}$$

and the slope k and intercept y were optimized. The LLEVAP model was used for these

simulations at high RH. The evaporation below the highest RH was simulated with the KM-GAP model. The best-fit VD (and ΔH_{vap} in **Paper IV**) was taken from the high RH optimization and only the viscosity contribution parameters b_i were optimized to yield simulated evapograms that match the measurements.

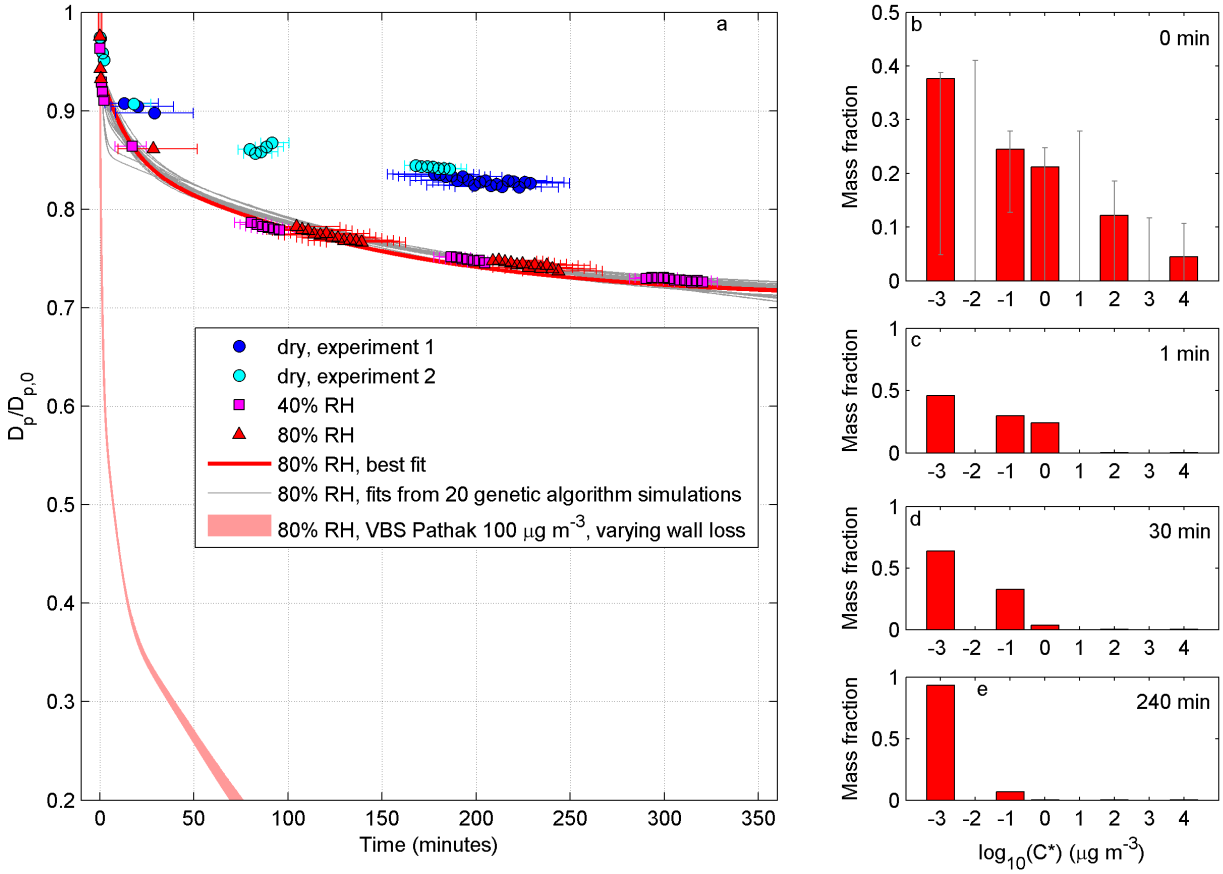

Figure 5.1: a) All the measured evapograms in **Paper III** and simulated evapograms for RH=80% experiments (red and gray lines). The light red area shows the evapogram simulated with the VD reported by Pathak et al. (2007). b) the particle phase VD at the start of the evaporation for the best fit VD (red bars) and the variation in mass fraction of each VD compound between 20 calculated VD estimates (whiskers) c–e) the time evolution of the best fit VD.

Figure 5.1a shows the measured and simulated evapograms for the evaporation mea-

sured at high RH in **Paper III**. The figure also shows the evapograms calculated using VD from Pathak et al. (2007) which was derived from growth measurements of SOA generated from the ozonolysis of α-pinene. The VD values derived by Pathak et al. (2007) are indicative of a clearly much faster rate of evaporation than that needed to explain the measured evapograms.

Figure 5.1b shows the initial VD that is needed for the LLEVAP model to reproduce the measurements and Fig. 5.1c–e show how the best fit VD evolves during the evaporation. Initially, around 40% of organic molecules are in the two least volatile VD compounds. This amount compares well to the VD estimated in **Paper IV** (Fig. 5.2a–b). The results are also comparable to the results of Wilson et al. (2015) which indicated that a significant fraction of non-volatile material would be needed to explain their isothermal evaporation measurements at high RH and also with recent findings of extremely low-volatility compounds in the gas phase (Ehn et al., 2014; Jokinen et al., 2015).

Paper IV reports the ΔH_{vap} for two different SOA systems. The derived vaporization enthalpies are shown in Fig. 5.2c–d. For the α-pinene + O_3 system the estimated ΔH_{vap} values are in a range ca. 50–130 kJ mol^{-1} and for the α-pinene + OH system from 1–150 kJ mol^{-1} which are in the same range as reported in other studies for α-pinene SOA (Saha and Grieshop, 2016; Epstein et al., 2009; Sheehan and Bowman, 2001; Bilde and Pandis, 2001) except for the very lowest values of α-pinene + OH system. However, the slope and the intercept obtained by Saha and Grieshop (2016) and Epstein et al. (2009) are not the same as the results of **Paper IV**. The reasons for these slight deviations are unknown. However, the ΔH_{vap} values in **Paper IV** are estimated only from two evaporation experiments. With more evaporation measurements at multiple different temperatures, the ΔH_{vap} could be characterized more accurately.

The evaporation of the α-pinene SOA at RH below or equal to 40% was studied in **Papers III–IV**. A representative set of results is shown in Fig. 5.3 (see also Fig. 2 in **Paper III**). In order to model the evaporation at 20%–40% RH throughout the experimental time scale, particle phase mass transfer limitations needed to be taken into account. Initially the evaporation of organic compounds is controlled by the VD (the solid and dashed lines overlap in Fig. 5.3) but once the compounds with the highest volatilities formed in the flow tube have evaporated, the evaporation becomes mass transfer limited.

These results of **Papers III–IV** differ from those of Wilson et al. (2015) who concluded

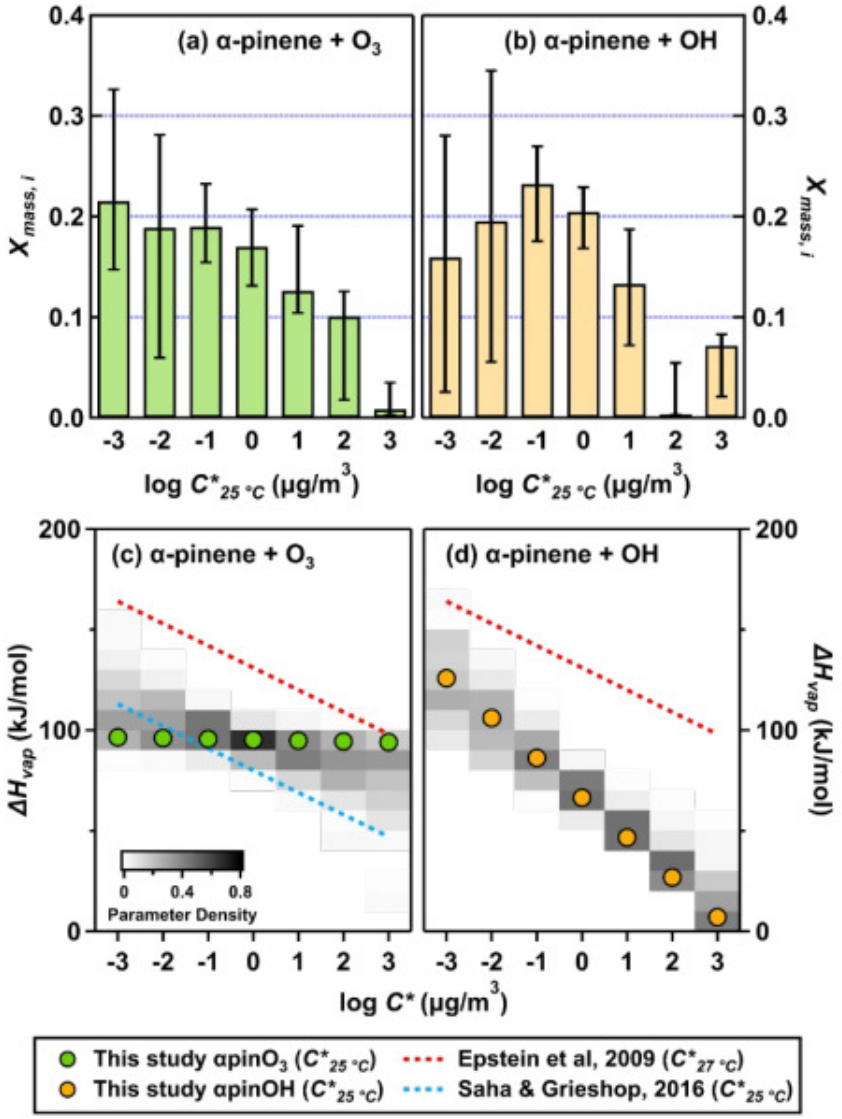

Figure 5.2: Estimated VD (a–b) and enthalpy of vaporization (c–d) from optimizing the LLEVAP model to produce similar evapograms as those measured at RH=80% for the evaporation of the two different α-pinene SOA systems studied in **Paper IV**. The bars in subfigures a–b and circles in c–d show the best-fit parameters. The parameter density shows the relative amount of estimates at a certain ΔH_{vap} value.

that the evaporation at RH=50% was similar to evaporation under dry conditions. In **Paper III**, it was speculated, that deviations in the mass loading when the SOA is formed could explain some of the discrepancy between these results. The SOA mass loading was high (in the order of 1000 μgm^{-3} in both **Papers III–IV**) which

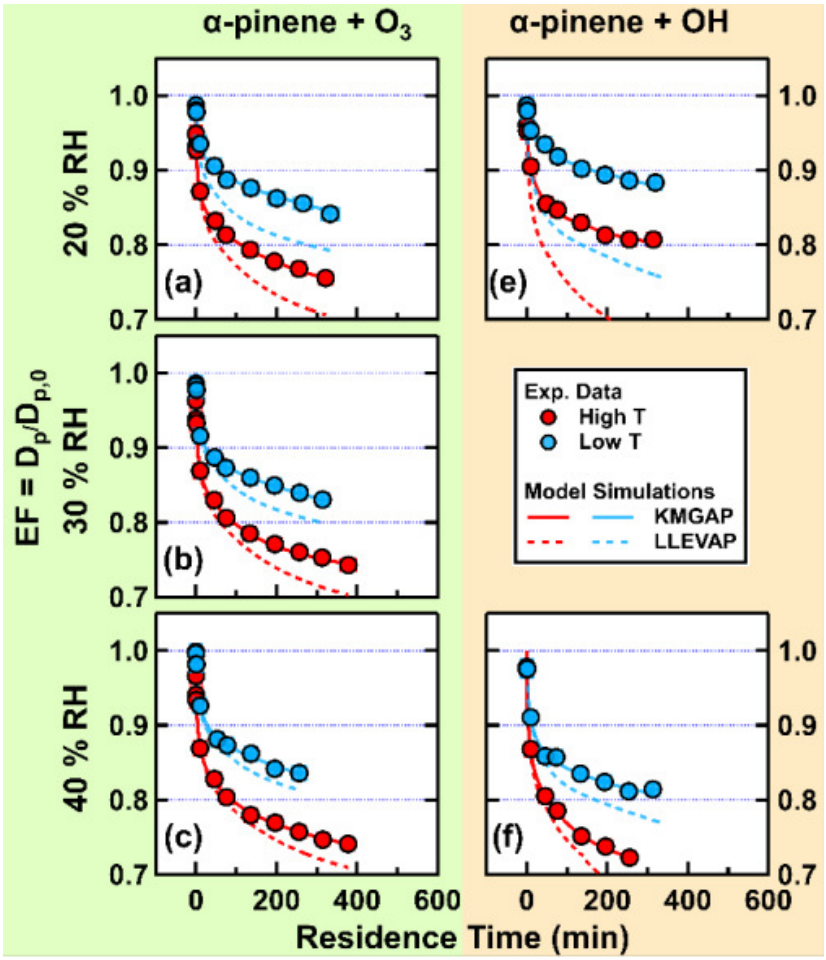

Figure 5.3: Measured and modelled evapograms for α-pinene ozonolysis (a–b) and α-pinene + OH (e–f) systems at different RH conditions. The solid lines are calculated by optimizing the particle phase viscosity such that the KM-GAP output matches the measurements. The dashed lines are calculated by taking the VD derived at RH=80% and changing only the simulation RH to the correct value.

allowed partitioning of high volatility compounds into the particle phase. These high volatility compounds can lower the viscosity of the particles during the early stages of the evaporation.

Based on the results obtained in **Papers III–IV** it can be said that the viscosity starts to hinder the evaporation of the α-pinene SOA particles studied in this thesis at around $\eta = 10^4$–10^5 Pa s. A strong composition dependency on the viscosity is needed as the viscosity in the simulations was between $\eta = 10^7$–10^8 at the end of the evaporation.

6 Hygroscopicity of dimethylamine containing particles

Dimethylamine (DMA) is an important organic compound that is emitted into the atmosphere from both anthropogenic and biogenic sources (Ge et al., 2011; VandenBoer et al., 2011; Youn et al., 2015). The particle phase amount of DMA is higher during the new particle formation events[5] (Mäkelä et al., 2001). DMA is also found in freshly nucleated particles (Smith et al., 2010) creating a need to test how well DMA properties are understood in current state-of-the-art thermodynamic models when particle curvature affects the simulated properties.

Paper V tested the ability of the E-AIM model (Wexler and Clegg, 2002) to simulate the laboratory measured values of hygroscopicity at sub-saturated conditions and with particle sizes where the Kelvin term (Eq. 2.2) would affect the water partitioning between the gas and the particle phases.

An example of results from **Paper V** is shown in Fig. 6.1. The hygroscopic growth of particles was measured with a nano-hygroscopicity tandem differential mobility analyzer (nano-HTDMA) (Keskinen et al., 2011; Kim et al., 2016). The experimental setup included also an Aerodyne Inc., Aerosol Mass specrometer (AMS) (Jayne et al., 2000), which revealed that the particle compositions differed from the nominal strengths of the solutions that were atomized to create the studied particles. In addition to dimethylamine, also ammonia (NH_3) was found in the particles. Fig. 6.1 shows two calculated Hygroscopic growth factor (GF) curves. The solid lines are calculated using the nominal DMA:SA ratio of the solution and the dashed lines are calculated using the AMS measured composition.

For larger dry particle sizes of 80 nm and 200 nm, hygroscopic growth factors (GF) calculated with the E-AIM model compared well with the experimental values (Fig. 6.1 c–d) when AMS measured particle composition was used as an input to the E-AIM model. The same cannot be said when the comparison was done for dry particle sizes 10 and 20 nm, where the GF calculated with the E-AIM model were smaller than their measured counterparts.

[5]growth of nanometer sized particles to sizes where they can impact climate. These events are observed all-around the world (Nieminen et al., 2018).

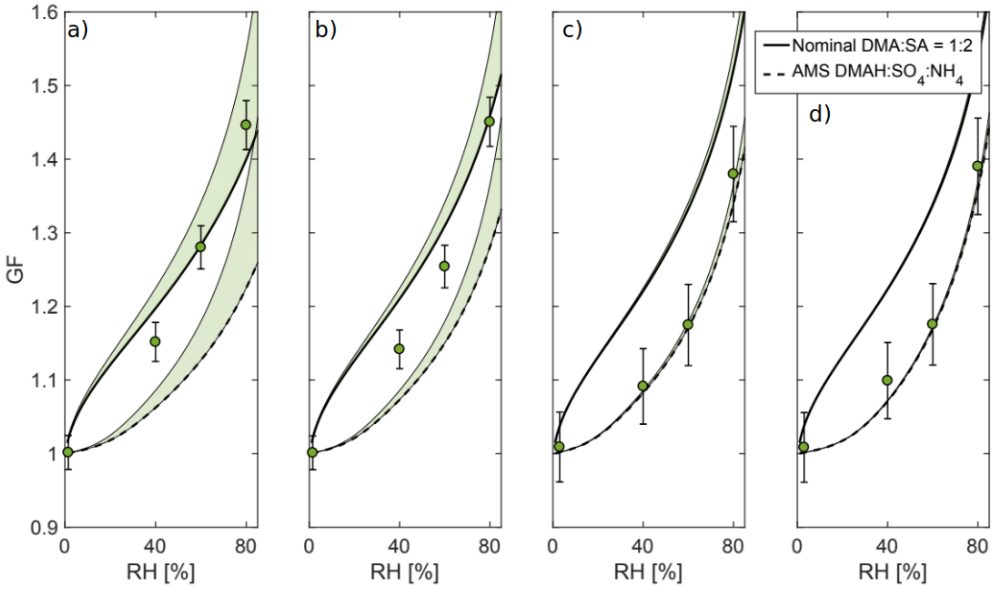

Figure 6.1: The measured and simulated hygroscopic growth factors (GF) at a nominal molar DMA:SA ratio 1:2 in **Paper V**. The solid line is calculated using the nominal DMA:SA molar ratio and the dashed line using composition measured with the AMS. The shaded regions represent the uncertainty of the simulated growth factors. Subfigures show the results for the following dry particle diameters a) 10 nm b) 20 nm c) 80 nm d) 200 nm

The AMS cannot directly measure the two smallest studied dry particle sizes, which leaves open the possibility that the smaller particles could be more acidic than the larger ones. The more acidic composition compared to the AMS measurements could explain the discrepancy between the measured and modelled values hygroscopicity. The inspection of hygroscopicity growth parameter κ (Petters and Kreidenweis, 2007) showed size-dependency, which would not be the case if the particles had the same composition at all dry particle sizes. This result indicated that the composition of the smallest particles could have differed from the other particles due to evaporation of basic compounds (DMA and ammonia) in the sampling lines.

In order to investigate the effect of base evaporation in detail, E-AIM was coupled with a dynamic particle growth model (MABNAG) (Yli-Juuti et al., 2013). The goal was to test how much of the basic compounds could evaporate and to determine whether the composition of the particles after evaporation produces the growth factors that were measured when used as an input to the E-AIM. The results revealed that even

at conditions that were maximally favorable for evaporation of the basic compounds in the sampling lines, the composition was not acidic enough to produce the measured hygroscopicity behavior. **Paper V** concluded that there are uncertainties in modeling the thermodynamics of DMA-containing particles, when the particle size is small enough for the Kelvin effect to play a role in gas–particle partitioning.

7 Review of papers and the author's contribution

Paper I presents a method to estimate volatility distribution and viscosity from isothermal particle evaporation data of organic aerosol. Both simulated and experimental data were used to determine the degree to which these properties can be estimated. I developed the version of the MCGA optimization algorithm used in this study, participated in planning the numerical test cases, performed the MCGA calculations and wrote the paper with contributions from all of the co-authors.

Paper II compares the volatility distributions estimated using the method described in **Paper I** and a method based on mass spectrometer data that utilizes the PMF method. I participated in planning the study, performed all the calculations with the exception of the PMF analysis and wrote the paper with contributions from all of the co-authors.

Paper III reports isothermal evaporation measurements of α-pinene derived SOA particles at three different RH conditions. The volatility distribution and viscosity of these particles were estimated with a process model optimization scheme similar to that presented in **Paper I**. I was responsible for developing and testing the optimization algorithm and performing the estimation of the VD from the evaporation data. I participated in writing the methods and interpreting the results.

Paper IV investigates isothermal evaporation of α-pinene derived SOA particles measured with a similar setup as described in **Paper III**. The novelty in the paper is that the measurements were performed at two different temperatures and the SOA was formed with two different oxidants. The measurements were analyzed with the process model optimization method presented in **Paper I**. I participated in the measurements, did all the estimations of VD, viscosity and enthalpy of vaporization, as well as contributing to the interpretation of the results and to the writing of the paper.

Paper V examined the hygroscopicity of dimethylamine containing particles at different RH conditions and particle sizes. The hygroscopicity measurements were compared to model results calculated with the E-AIM model. I performed the model calculations, participated in data analysis as well as in the interpretation of the results and wrote the paper as one of the two first authors.

8 Conclusions

This thesis studied the characterization of organic aerosol properties by utilizing process modelling. The volatility distribution and viscosity of organic aerosols, and in detail, the SOA produced from the oxidation of α-pinene and methods to estimate these parameters using process modelling techniques and global optimization were studied. The hygroscopicity of DMA-containing organic aerosols and the capability of a state-of-the-art thermodynamic equilibrium model to predict the hygroscopicity were also examined. Below, the findings in this thesis are summarized with respect to the aims presented in Sect. 1.3.

The process model optimization method described and tested in **Paper I** is a promising method to quantify the volatility distribution of organic compounds and the particle phase mass transfer limitations from isothermal evaporation experiments. However, care has to be taken when the method is applied. The method might not be applicable in the presence of too small amounts of data, because there may be too many possible combinations for the estimated properties that reproduce the measurements when used as an input to process model. Furthermore, it should be kept in mind that the estimated properties are influenced by the processes that are or are not taken into account in the process models themselves.

Paper II compared the volatility distribution of organic compounds obtained using the method in **Paper I** to the volatility distribution calculated from FIGAERO-CIMS measurements using the PMF method. The volatility distributions obtained from evaporation measurements showed similarities when the volatility of each PMF factor was interpreted to be a range of possible values rather than a single value. Combining the FIGAERO-CIMS data to a characterization of the properties of the SOA with process models was considered to be an interesting addition when SOA properties are estimated from isothermal evaporation experiments, since the data constrains the volatility distribution more than the particle size change data alone.

The volatility distribution of SOA produced from oxidation of α-pinene was estimated in **Papers III–IV** by applying the process model optimization method to particle size change data during isothermal particle evaporation. In order to produce similar simulated evapograms as those that had been measured, a significant fraction (ca. 40% by molecule number at the start of the evaporation) of the organics had to have effective saturation mass concentration below or equal to 10^{-2} μgm^{-3}, which is consistent with

the current knowledge of the oxidation products of monoterpenes (Ehn et al., 2014; Jokinen et al., 2015) and qualitatively to the results reported by other investigators examining the isothermal evaporation of α-pinene (Wilson et al., 2015).

The mass transfer limitations need to be taken into account when modelling SOA dynamics at RH below or equal to 40%. The results obtained in **Papers III–IV** revealed that the particle phase viscosity started to affect the evaporation once the compounds with the highest volatility had evaporated from the particle phase. The threshold viscosity where the particle phase mass transfer limitations started to matter for 80 nm SOA particles studied in this thesis was quantified to be 10^4–10^5 Pa s. However, as 40% RH is at the lower end of typical ambient RH, it seems that the volatility of the organic compounds influence the particle dynamics probably more than the mass transfer limitations.

The isothermal evaporation of α-pinene SOA at two different temperatures studied in **Paper IV** showed that in order to model the evaporation correctly at these two temperatures, enthalpies of vaporization between 1–150 kJ mol^{-1} were needed.

The results of **Paper V** revealed that there exists uncertainties in thermodynamic properties of DMA as a state-of-the-art thermodynamic equilibrium model was unable to predict the hygroscopicity of DMA containing particles when the particle size was in the order of a few tens of nanometers.

From the modelling point-of-view there are several issues that could be investigated in the future. To analyze multiple data sets accurately with the process model optimization method, the non-ideality of the particle phase needs to be taken into account. If the non-ideality is not considered, the properties that are estimated using measurements from one set of evaporation conditions might not produce the correct measured evapogram at other evaporation conditions. If multiple data sets are analyzed simultaneously and the non-ideality is not taken into account, the process model optimization might not be able to produce accurate estimates for the studied properties.

A good starting point could be to include the activity coefficient of water, but ultimately the activity coefficients of the other (VD) compounds could also be incorporated. The non-ideality could also be taken into account when modelling the viscosity of organic aerosol as was done in the recent study by Gervasi et al. (2019).

Future evaporation studies could concentrate on measuring the evaporation of SOA

at very low temperatures and with multiple precursors to further quantify the SOA dynamics throughout the atmosphere. These measurements should be done at as many different temperatures as possible to help quantify the effect of temperature on both volatility and viscosity. Future evaporation studies should include modelling of the evaporation process and report a volatility distribution estimated, for example, with the process model optimization method described and tested in this thesis.

As DMA is an important constituent of atmospheric particles even on the nanometer scale (Loukonen et al., 2010; Kurtén et al., 2008; Mäkelä et al., 2001) further investigation are needed to clarify the thermodynamic properties of DMA-containing solutions. Based on the results emerging from this thesis, the composition and hence the hygroscopicity of DMA-containing particles with diameters in the rage of few tens of nanometers is not correctly predicted with a state-of-the-art thermodynamic equilibrium model. Further laboratory experiments should include measurements of the particle phase composition as this can differ significantly from the nominal strengths of solutions that are atomized.

References

Abramson, E., Imre, D., Beránek, J., Wilson, J., and Zelenyuk, A. (2013). Experimental determination of chemical diffusion within secondary organic aerosol particles. *Phys. Chem. Chem. Phys.*, 15(8):2983–2991.

Almeida, J., Schobesberger, S., Kürten, A., Ortega, I. K., Kupiainen-Määttä, O., Praplan, A. P., Adamov, A., Amorim, A., Bianchi, F., Breitenlechner, M., David, A., Dommen, J., Donahue, N. M., Downard, A., Dunne, E., Duplissy, J., Ehrhart, S., Flagan, R. C., Franchin, A., Guida, R., Hakala, J., Hansel, A., Heinritzi, M., Henschel, H., Jokinen, T., Junninen, H., Kajos, M., Kangasluoma, J., Keskinen, H., Kupc, A., Kurtén, T., Kvashin, A. N., Laaksonen, A., Lehtipalo, K., Leiminger, M., Leppä, J., Loukonen, V., Makhmutov, V., Mathot, S., McGrath, M. J., Nieminen, T., Olenius, T., Onnela, A., Petäjä, T., Riccobono, F., Riipinen, I., Rissanen, M., Rondo, L., Ruuskanen, T., Santos, F. D., Sarnela, N., Schallhart, S., Schnitzhofer, R., Seinfeld, J. H., Simon, M., Sipilä, M., Stozhkov, Y., Stratmann, F., Tomé, A., Tröstl, J., Tsagkogeorgas, G., Vaattovaara, P., Viisanen, Y., Virtanen, A., Vrtala, A., Wagner, P. E., Weingartner, E., Wex, H., Williamson, C., Wimmer, D., Ye, P., Yli-Juuti, T., Carslaw, K. S., Kulmala, M., Curtius, J., Baltensperger, U., Worsnop, D. R., Vehkamäki, H., and Kirkby, J. (2013). Molecular understanding of sulphuric acid–amine particle nucleation in the atmosphere. *Nature*, 502(7471):359–363.

Atkinson, R. and Arey, J. (2003). Atmospheric Degradation of Volatile Organic Compounds. *Chem. Rev.*, 103(12):4605–4638.

Bäck, J., Aalto, J., Henriksson, M., Hakola, H., He, Q., and Boy, M. (2012). Chemodiversity of a Scots pine stand and implications for terpene air concentrations. *Biogeosciences*, 9(2):689–702.

Berkemeier, T., Ammann, M., Krieger, U. K., Peter, T., Spichtinger, P., Pöschl, U., Shiraiwa, M., and Huisman, A. J. (2017). Technical note: Monte Carlo genetic algorithm (MCGA) for model analysis of multiphase chemical kinetics to determine transport and reaction rate coefficients using multiple experimental data sets. *Atmos. Chem. Phys.*, 17(12):8021–8029.

Bilde, M., Barsanti, K., Booth, M., Cappa, C. D., Donahue, N. M., Emanuelsson, E. U., McFiggans, G., Krieger, U. K., Marcolli, C., Topping, D., Ziemann, P., Barley, M., Clegg, S., Dennis-Smither, B., Hallquist, M., Hallquist, t. M., Khlystov, A.,

Kulmala, M., Mogensen, D., Percival, C. J., Pope, F., Reid, J. P., V Ribeiro da Silva, M. A., Rosenoern, T., Salo, K., Pia Soonsin, V., Yli-Juuti, T., Prisle, N. L., Pagels, J., Rarey, J., Zardini, A. A., and Riipinen, I. (2015). Saturation Vapor Pressures and Transition Enthalpies of Low- Volatility Organic Molecules of Atmospheric Relevance: From Dicarboxylic Acids to Complex Mixtures. *Chem. Rev*, 115:4115–4156.

Bilde, M. and Pandis, S. N. (2001). Evaporation Rates and Vapor Pressures of Individual Aerosol Species Formed in the Atmospheric Oxidation of α- and β-Pinene. *Environ. Sci. Technol.*, 35(16):3344–3349.

Buchholz, A., Lambe, A. T., Ylisirniö, A., Li, Z., Tikkanen, O.-P., Faiola, C., Kari, E., Hao, L., Luoma, O., Huang, W., Mohr, C., Worsnop, D. R., Nizkorodov, S. A., Yli-Juuti, T., Schobesberger, S., and Virtanen, A. (2019a). Insights into the O:C-dependent mechanisms controlling the evaporation of α-pinene secondary organic aerosol particles. *Atmos. Chem. Phys.*, 19(6):4061–4073.

Buchholz, A., Ylisirniö, A., Huang, W., Mohr, C., Canagaratna, M., Worsnop, D. R., Schobesberger, S., and Virtanen, A. (2019b). Deconvolution of FIGAERO-CIMS thermal desorption profiles using positive matrix factorisation to identify chemical and physical processes during particle evaporation. *Atmos. Chem. Phys. Discuss.* in review.

Clegg, S. L., Brimblecombe, P., and Wexler, A. S. (1998). Thermodynamic Model of the System H^+ - NH_4^+ - SO_4^{2-} - NO_3^- - H_2O at Tropospheric Temperatures. *J. Phys. Chem. A*, 102(12):2137–2154.

Clegg, S. L., Pitzer, K. S., and Brimblecombe, P. (1992). Thermodynamics of Multicomponent, Miscible, Ionic Solutions. 2. Mlxtures Including Unsymmetrical Electrolytes. *J. Phys. Chem. A*, 96(23):9470–9479.

Clegg, S. L., Seinfeld, J. H., and Brimblecombe, P. (2001). Thermodynamic modelling of aqueous aerosols containing electrolytes and dissolved organic compounds. *J. Aerosol Sci.*, 32(6):713–738.

Clegg, S. L. and Wexler, A. S. (2011). Densities and Apparent Molar Volumes of Atmospherically Important Electrolyte Solutions. 2. The Systems over the Entire Concentration Range. *J. Phys. Chem. A*, 115(15):3461–3474.

D'Ambro, E. L., Schobesberger, S., Zaveri, R. A., Shilling, J. E., Lee, B. H., Lopez-Hilfiker, F. D., Mohr, C., and Thornton, J. A. (2018). Isothermal Evaporation of α-Pinene Ozonolysis SOA: Volatility, Phase State, and Oligomeric Composition. *ACS Earth Space Chem.*, 2(10):1058–1067.

Davies, J. F., Haddrell, A. E., Rickards, A. M. J., and Reid, J. P. (2013). Simultaneous Analysis of the Equilibrium Hygroscopicity and Water Transport Kinetics of Liquid Aerosol. *Anal. Chem.*, 85(12):5819–5826.

DeRieux, W.-S. W., Li, Y., Lin, P., Laskin, J., Laskin, A., Bertram, A. K., Nizkorodov, S. A., and Shiraiwa, M. (2018). Predicting the glass transition temperature and viscosity of secondary organic material using molecular composition. *Atmos. Chem. Phys.*, 18(9):6331–6351.

Donahue, N. M., Robinson, a. L., Stanier, C. O., and Pandis, S. N. (2006). Coupled partitioning, dilution, and chemical aging of semivolatile organics. *Environ. Sci. Technol.*, 40(8):2635–2643.

Dunne, E. M., Gordon, H., Kürten, A., Almeida, J., Duplissy, J., Williamson, C., Ortega, I. K., Pringle, K. J., Adamov, A., Baltensperger, U., Barmet, P., Benduhn, F., Bianchi, F., Breitenlechner, M., Clarke, A., Curtius, J., Dommen, J., Donahue, N. M., Ehrhart, S., Flagan, R. C., Franchin, A., Guida, R., Hakala, J., Hansel, A., Heinritzi, M., Jokinen, T., Kangasluoma, J., Kirkby, J., Kulmala, M., Kupc, A., Lawler, M. J., Lehtipalo, K., Makhmutov, V., Mann, G., Mathot, S., Merikanto, J., Miettinen, P., Nenes, A., Onnela, A., Rap, A., Reddington, C. L. S., Riccobono, F., Richards, N. A. D., Rissanen, M. P., Rondo, L., Sarnela, N., Schobesberger, S., Sengupta, K., Simon, M., Sipilä, M., Smith, J. N., Stozkhov, Y., Tomé, A., Tröstl, J., Wagner, P. E., Wimmer, D., Winkler, P. M., Worsnop, D. R., and Carslaw, K. S. (2016). Global atmospheric particle formation from CERN CLOUD measurements. *Science*, 354(6316):1119–1124.

Dusek, U., Frank, G., Hildebrandt, L., Curtius, J., Schneider, J., Walter, S., Chand, D., Drewnick, F., Hings, S., Jung, D., et al. (2006). Size matters more than chemistry for cloud-nucleating ability of aerosol particles. *Science*, 312(5778):1375–1378.

Dutcher, C. S., Wexler, A. S., and Clegg, S. L. (2010). Surface Tensions of Inorganic Multicomponent Aqueous Electrolyte Solutions and Melts. *J. Phys. Chem. A*, 114(46):12216–12230.

Eberhart, R. and Kennedy, J. (1995). A new optimizer using particle swarm theory. In *MHS'95. Proceedings of the Sixth International Symposium on Micro Machine and Human Science*, pages 39–43.

Ehn, M., Thornton, J. A., Kleist, E., Sipilä, M., Junninen, H., Pullinen, I., Springer, M., Rubach, F., Tillmann, R., Lee, B., Lopez-Hilfiker, F., Andres, S., Acir, I.-H., Rissanen, M., Jokinen, T., Schobesberger, S., Kangasluoma, J., Kontkanen, J., Nieminen, T., Kurtén, T., Nielsen, L. B., Jørgensen, S., Kjaergaard, H. G., Canagaratna, M., Maso, M. D., Berndt, T., Petäjä, T., Wahner, A., Kerminen, V.-M., Kulmala, M., Worsnop, D. R., Wildt, J., and Mentel, T. F. (2014). A large source of low-volatility secondary organic aerosol. *Nature*, 506(7489):476–479.

Einstein, A. (1905). Über die von der molekularkinetischen Theorie der Wärme geforderte Bewegung von in ruhenden Flüssigkeiten suspendierten Teilchen. *Annalen der Physik*, 322(8):549–560.

EPA (2011). Exposure factors handbook: 2011 edition. Technical report, EPA (Environmental Protection Agency), U.S.

Epstein, S. A., Riipinen, I., and Donahue, N. M. (2009). A Semiempirical Correlation between Enthalpy of Vaporization and Saturation Concentration for Organic Aerosol. *Environ. Sci. Technol.*, 44(2):743–748.

Franklin, M., Zeka, A., and Schwartz, J. (2007). Association between $PM_{2.5}$ and all-cause and specific-cause mortality in 27 US communities. *J. Expo. Sci. Environ. Epidemiol.*, 17(3):279–287.

Fredenslund, A., Jones, R. L., and Prausnitz, J. M. (1975). Group-contribution estimation of activity coefficients in nonideal liquid mixtures. *AIChE Journal*, 21(6):1086–1099.

Fuchs, N. A. and Sutugin, A. G. (1971). HIGH-DISPERSED AEROSOLS. In Hidy, G. M. and Brock, J. R., editors, *Topics in Current Aerosol Research*, International Reviews in Aerosol Physics and Chemistry, page 1. Pergamon.

Ge, X., Wexler, A. S., and Clegg, S. L. (2011). Atmospheric amines Part I . A review. *Atmospheric Environ.*, 45:524–546.

Gervasi, N. R., Topping, D. O., and Zuend, A. (2019). A predictive group-contribution model for the viscosity of aqueous organic aerosol. *Atmos. Chem. Phys. Discuss.* in review.

Glantschnig, W. J. and Chen, S.-H. (1981). Light scattering from water droplets in the geometrical optics approximation. *Appl. Opt.*, 20(14):2499.

Glasius, M. and Goldstein, A. H. (2016). Recent Discoveries and Future Challenges in Atmospheric Organic Chemistry. *Environ. Sci. Technol.*, 50(6):2754–2764.

Goldberg, D. E. (1989). *Genetic Algorithms in Search, Optimization and Machine Learning*. Addison-Wesley Longman Publishing Co., Inc., Boston, MA, USA, 1st edition.

Goldstein, A. H. and Galbally, I. E. (2007). Known and Unexplored Organic Constituents in the Earth's Atmosphere. *Environ. Sci. Technol.*, 41(5):1514–1521.

Grieshop, A. P., Donahue, N. M., and Robinson, A. L. (2007). Is the gas-particle partitioning in alpha-pinene secondary organic aerosol reversible? *Geophys. Res. Lett.*, 34(14).

Guenther, A. B., Jiang, X., Heald, C. L., Sakulyanontvittaya, T., Duhl, T., Emmons, L. K., and Wang, X. (2012). The Model of Emissions of Gases and Aerosols from Nature version 2.1 (MEGAN2.1): An extended and updated framework for modeling biogenic emissions. *Geosci. Model Dev.*, 5(6):1471–1492.

Hallquist, M., Wenger, J. C., Baltensperger, U., Rudich, Y., Simpson, D., Claeys, M., Dommen, J., Donahue, N. M., George, C., Goldstein, A. H., Hamilton, J. F., Herrmann, H., Hoffmann, T., Iinuma, Y., Jang, M., Jenkin, M. E., Jimenez, J. L., Kiendler-Scharr, A., Maenhaut, W., McFiggans, G., Mentel, T. F., Monod, A., Prévôt, A. S. H., Seinfeld, J. H., Surratt, J. D., Szmigielski, R., and Wildt, J. (2009). The formation, properties and impact of secondary organic aerosol: Current and emerging issues. *Atmos. Chem. Phys.*, 9(14):5155–5236.

Hansen, H. K., Rasmussen, P., Fredenslund, A., Schiller, M., and Gmehling, J. (1991). Vapor-liquid equilibria by UNIFAC group contribution. 5. Revision and extension. *Ind. Eng. Chem. Res.*, 30(10):2352–2355.

Järvinen, E., Ignatius, K., Nichman, L., Kristensen, T. B., Fuchs, C., Hoyle, C. R., Höppel, N., Corbin, J. C., Craven, J., Duplissy, J., Ehrhart, S., El Haddad, I., Frege,

C., Gordon, H., Jokinen, T., Kallinger, P., Kirkby, J., Kiselev, A., Naumann, K.-H., Petäjä, T., Pinterich, T., Prevot, A. S. H., Saathoff, H., Schiebel, T., Sengupta, K., Simon, M., Slowik, J. G., Tröstl, J., Virtanen, A., Vochezer, P., Vogt, S., Wagner, A. C., Wagner, R., Williamson, C., Winkler, P. M., Yan, C., Baltensperger, U., Donahue, N. M., Flagan, R. C., Gallagher, M., Hansel, A., Kulmala, M., Stratmann, F., Worsnop, D. R., Möhler, O., Leisner, T., and Schnaiter, M. (2016). Observation of viscosity transition in α-pinene secondary organic aerosol. *Atmos. Chem. Phys.*, 16(7):4423–4438.

Jayne, J. T., Leard, D. C., Zhang, X., Davidovits, P., Smith, K. A., Kolb, C. E., and Worsnop, D. R. (2000). Development of an Aerosol Mass Spectrometer for Size and Composition Analysis of Submicron Particles. *Aerosol Sci. Tech.*, 33(1-2):49–70.

Jimenez, J. L., Canagaratna, M. R., Donahue, N. M., Prevot, A. S. H., Zhang, Q., Kroll, J. H., DeCarlo, P. F., Allan, J. D., Coe, H., Ng, N. L., Aiken, A. C., Docherty, K. S., Ulbrich, I. M., Grieshop, A. P., Robinson, A. L., Duplissy, J., Smith, J. D., Wilson, K. R., Lanz, V. A., Hueglin, C., Sun, Y. L., Tian, J., Laaksonen, A., Raatikainen, T., Rautiainen, J., Vaattovaara, P., Ehn, M., Kulmala, M., Tomlinson, J. M., Collins, D. R., Cubison, M. J., Dunlea, E. J., Huffman, J. A., Onasch, T. B., Alfarra, M. R., Williams, P. I., Bower, K., Kondo, Y., Schneider, J., Drewnick, F., Borrmann, S., Weimer, S., Demerjian, K., Salcedo, D., Cottrell, L., Griffin, R., Takami, A., Miyoshi, T., Hatakeyama, S., Shimono, A., Sun, J. Y., Zhang, Y. M., Dzepina, K., Kimmel, J. R., Sueper, D., Jayne, J. T., Herndon, S. C., Trimborn, A. M., Williams, L. R., Wood, E. C., Middlebrook, A. M., Kolb, C. E., Baltensperger, U., Worsnop, D. R., and Worsnop, D. R. (2009). Evolution of organic aerosols in the atmosphere. *Science*, 326(5959):1525–9.

Jokinen, T., Berndt, T., Makkonen, R., Kerminen, V.-M., Junninen, H., Paasonen, P., Stratmann, F., Herrmann, H., Guenther, A. B., Worsnop, D. R., Kulmala, M., Ehn, M., and Sipilä, M. (2015). Production of extremely low volatile organic compounds from biogenic emissions: Measured yields and atmospheric implications. *Proc. Natl. Acad. Sci. U.S.A.*, 112(23):7123–7128.

Julin, J., Winkler, P. M., Donahue, N. M., Wagner, P. E., and Riipinen, I. (2014). Near-Unity Mass Accommodation Coefficient of Organic Molecules of Varying Structure. *Environ. Sci. Technol.*, 48(20):12083–12089.

Kang, E., Root, M. J., Toohey, D. W., and Brune, W. H. (2007). Introducing the concept of potential aerosol mass (PAM). *Atmos. Chem. Phys.*, 7(22):5727–5744.

Keskinen, H., Romakkaniemi, S., Jaatinen, A., Miettinen, P., Saukko, E., Jorma, J., Makela, J. M., Virtanen, A., Smith, J. N., and Laaksonen, A. (2011). On-Line Characterization of Morphology and Water Adsorption on Fumed Silica Nanoparticles. *Aerosol Sci. Tech.*, 45(12):1441–1447.

Kim, J., Ahlm, L., Yli-Juuti, T., Lawler, M., Keskinen, H., Tröstl, J., Schobesberger, S., Duplissy, J., Amorim, A., Bianchi, F., Donahue, N. M., Flagan, R. C., Hakala, J., Heinritzi, M., Jokinen, T., Kürten, A., Laaksonen, A., Lehtipalo, K., Miettinen, P., Petäjä, T., Rissanen, M. P., Rondo, L., Sengupta, K., Simon, M., Tomé, A., Williamson, C., Wimmer, D., Winkler, P. M., Ehrhart, S., Ye, P., Kirkby, J., Curtius, J., Baltensperger, U., Kulmala, M., Lehtinen, K. E. J., Smith, J. N., Riipinen, I., and Virtanen, A. (2016). Hygroscopicity of nanoparticles produced from homogeneous nucleation in the CLOUD experiments. *Atmos. Chem. Phys.*, 16(1):293–304.

Koop, T., Bookhold, J., Shiraiwa, M., and Pöschl, U. (2011). Glass transition and phase state of organic compounds: Dependency on molecular properties and implications for secondary organic aerosols in the atmosphere. *Phys. Chem. Chem. Phys.*, 13(43):19238–19255.

Kroll, J. H. and Seinfeld, J. H. (2008). Chemistry of secondary organic aerosol: Formation and evolution of low-volatility organics in the atmosphere. *Atmospheric Environ.*, 42(16):3593–3624.

Kuang, C., Riipinen, I., Sihto, S.-L., Kulmala, M., McCormick, A. V., and McMurry, P. H. (2010). An improved criterion for new particle formation in diverse atmospheric environments. *Atmos. Chem. Phys.*, 10(17):8469–8480.

Kulmala, M., Pirjola, L., and Mäkelä, J. M. (2000). Stable sulphate clusters as a source of new atmospheric particles. *Nature*, 404(6773):66–69.

Kulmala, M., Vehkamäki, H., Petäjä, T., Dal Maso, M., Lauri, A., Kerminen, V.-M., Birmili, W., and McMurry, P. (2004). Formation and growth rates of ultrafine atmospheric particles: A review of observations. *J. Aerosol Sci.*, 35(2):143–176.

Kulmala, M., Vesala, T., Schwarz, J., and Smolik, J. (1995). Mass transfer from a drop—II. Theoretical analysis of temperature dependent mass flux correlation. *Int. J. Heat Mass Transf.*, 38(9):1705–1708.

Kurtén, T., Loukonen, V., Vehkamäki, H., and Kulmala, M. (2008). Amines are likely to enhance neutral and ion-induced sulfuric acid-water nucleation in the atmosphere more effectively than ammonia. *Atmos. Chem. Phys.*, 8(14):4095–4103.

Laaksonen, A., Kulmala, M., O'Dowd, C. D., Joutsensaari, J., Vaattovaara, P., Mikkonen, S., Lehtinen, K. E. J., Sogacheva, L., Maso, M. D., Aalto, P., Petäjä, T., Sogachev, A., Yoon, Y. J., Lihavainen, H., Nilsson, D., Facchini, M. C., Cavalli, F., Fuzzi, S., Hoffmann, T., Arnold, F., Hanke, M., Sellegri, K., Umann, B., Junkermann, W., Coe, H., Allan, J. D., Alfarra, M. R., Worsnop, D. R., Riekkola, M.-L., Hyötyläinen, T., and Viisanen, Y. (2008). The role of VOC oxidation products in continental new particle formation. *Atmos. Chem. Phys.*, 8(10):2657–2665.

Lambe, A. T., Ahern, A. T., Williams, L. R., Slowik, J. G., Wong, J. P. S., Abbatt, J. P. D., Brune, W. H., Ng, N. L., Wright, J. P., Croasdale, D. R., Worsnop, D. R., Davidovits, P., and Onasch, T. B. (2011). Characterization of aerosol photooxidation flow reactors: Heterogeneous oxidation, secondary organic aerosol formation and cloud condensation nuclei activity measurements. *Atmos. Meas. Tech.*, 4(3):445–461.

Lee, B. H., Lopez-Hilfiker, F. D., Mohr, C., Kurtén, T., Worsnop, D. R., and Thornton, J. A. (2014). An Iodide-Adduct High-Resolution Time-of-Flight Chemical-Ionization Mass Spectrometer: Application to Atmospheric Inorganic and Organic Compounds. *Environ. Sci. Technol.*, 48(11):6309–6317.

Lehtinen, K. E. J. and Kulmala, M. (2003). A model for particle formation and growth in the atmosphere with molecular resolution in size. *Atmos. Chem. Phys.*, (3):251–257.

Liu, P., Li, Y. J., Wang, Y., Gilles, M. K., Zaveri, R. A., Bertram, A. K., and Martin, S. T. (2016). Lability of secondary organic particulate matter. *Proc. Natl. Acad. Sci. U.S.A.*, 113(45):12643–12648.

Löndahl, J., Pagels, J., Swietlicki, E., Zhou, J., Ketzel, M., Massling, A., and Bohgard, M. (2006). A set-up for field studies of respiratory tract deposition of fine and ultrafine particles in humans. *J. Aerosol Sci.*, 37(9):1152–1163.

Lopez-Hilfiker, F. D., Mohr, C., Ehn, M., Rubach, F., Kleist, E., Wildt, J., Mentel, T. F., Lutz, A., Hallquist, M., Worsnop, D., and Thornton, J. A. (2014). A novel

method for online analysis of gas and particle composition: Description and evaluation of a Filter Inlet for Gases and AEROsols (FIGAERO). *Atmos. Meas. Tech.*, 7(4):983–1001.

Loukonen, V., Kurtén, T., Ortega, I. K., Vehkamäki, H., Pádua, A. A. H., Sellegri, K., and Kulmala, M. (2010). Enhancing effect of dimethylamine in sulfuric acid nucleation in the presence of water – a computational study. *Atmos. Chem. Phys. Atmospheric Chemistry and Physics*, 10:4961–4974.

Mäkelä, J. M., Yli-Koivisto, S., Hiltunen, V., Seidl, W., Swietlicki, E., Teinilä, K., Sillanpää, M., Koponen, I. K., Paatero, J., Rosman, K., and Hämeri, K. (2001). Chemical composition of aerosol during particle formation events in boreal forest. *Tellus B*, 53(4):380–393.

Marsh, A., Miles, R. E. H., Rovelli, G., Cowling, A. G., Nandy, L., Dutcher, C. S., and Reid, J. P. (2017). Influence of organic compound functionality on aerosol hygroscopicity: Dicarboxylic acids, alkyl-substituents, sugars and amino acids. *Atmos. Chem. Phys.*, 17(9):5583–5599.

Meille, S. V., Allegra, G., Geil, P. H., He, J., Hess, M., Jin, J.-I., Kratochvíl, P., Mormann, W., and Stepto, R. (2011). Definitions of terms relating to crystalline polymers (IUPAC Recommendations 2011). *Pure Appl. Chem.*, 83(10):1831–1871.

Miller, C. C. (1924). The Stokes-Einstein law for diffusion in solution. *Proc. Royal Soc. Lond.*, 106(740):724–749.

Nieminen, T., Kerminen, V.-M., Petäjä, T., Aalto, P. P., Arshinov, M., Asmi, E., Baltensperger, U., Beddows, D. C. S., Beukes, J. P., Collins, D., Ding, A., Harrison, R. M., Henzing, B., Hooda, R., Hu, M., Hõrrak, U., Kivekäs, N., Komsaare, K., Krejci, R., Kristensson, A., Laakso, L., Laaksonen, A., Leaitch, W. R., Lihavainen, H., Mihalopoulos, N., Németh, Z., Nie, W., O'Dowd, C., Salma, I., Sellegri, K., Svenningsson, B., Swietlicki, E., Tunved, P., Ulevicius, V., Vakkari, V., Vana, M., Wiedensohler, A., Wu, Z., Virtanen, A., and Kulmala, M. (2018). Global analysis of continental boundary layer new particle formation based on long-term measurements. *Atmos. Chem. Phys.*, 18(19):14737–14756.

O'Meara, S., Topping, D. O., and McFiggans, G. (2016). The rate of equilibration of viscous aerosol particles. *Atmos. Chem. Phys.*, 16(8):5299–5313.

Paatero, P. and Tapper, U. (1994). Positive matrix factorization: A non-negative factor model with optimal utilization of error estimates of data values. *Environmetrics*, 5(2):111–126.

Pathak, R. K., Presto, A. A., Lane, T. E., Stanier, C. O., Donahue, N. M., and Pandis, S. N. (2007). Ozonolysis of α-pinene: Parameterization of secondary organic aerosol mass fraction. *Atmos. Chem. Phys.*, 7(14):3811–3821.

Petters, M. D. and Kreidenweis, S. M. (2007). A single parameter representation of hygroscopic growth and cloud condensation nucleus activity. *Atmos. Chem. Phys.*, 7(8):1961–1971.

Price, H., Mattsson, J., Zhang, Y., K. Bertram, A., F. Davies, J., W. Grayson, J., T. Martin, S., O'Sullivan, D., P. Reid, J., J. Rickards, A. M., and J. Murray, B. (2015). Water diffusion in atmospherically relevant α-pinene secondary organic material. *Chem. Sci.*, 6(8):4876–4883.

Reid, J. P., Bertram, A. K., Topping, D. O., Laskin, A., Martin, S. T., Petters, M. D., Pope, F. D., and Rovelli, G. (2018). The viscosity of atmospherically relevant organic particles. *Nat. Commun.*, 9(1):956.

Renbaum-Wolff, L., Grayson, J. W., Bateman, A. P., Kuwata, M., Sellier, M., Murray, B. J., Shilling, J. E., Martin, S. T., and Bertram, A. K. (2013). Viscosity of α-pinene secondary organic material and implications for particle growth and reactivity. *Proc. Natl. Acad. Sci. U.S.A.*, 110(20):8014–8019.

Riccobono, F., Schobesberger, S., Scott, C. E., Dommen, J., Ortega, I. K., Rondo, L., Almeida, J., Amorim, A., Bianchi, F., Breitenlechner, M., David, A., Downard, A., Dunne, E. M., Duplissy, J., Ehrhart, S., Flagan, R. C., Franchin, A., Hansel, A., Junninen, H., Kajos, M., Keskinen, H., Kupc, A., Kürten, A., Kvashin, A. N., Laaksonen, A., Lehtipalo, K., Makhmutov, V., Mathot, S., Nieminen, T., Onnela, A., Petäjä, T., Praplan, A. P., Santos, F. D., Schallhart, S., Seinfeld, J. H., Sipilä, M., Spracklen, D. V., Stozhkov, Y., Stratmann, F., Tomé, A., Tsagkogeorgas, G., Vaattovaara, P., Viisanen, Y., Vrtala, A., Wagner, P. E., Weingartner, E., Wex, H., Wimmer, D., Carslaw, K. S., Curtius, J., Donahue, N. M., Kirkby, J., Kulmala, M., Worsnop, D. R., and Baltensperger, U. (2014). Oxidation Products of Biogenic Emissions Contribute to Nucleation of Atmospheric Particles. *Science*, 344(6185):717–721.

Riipinen, I., Pierce, J., and Yli-Juuti, T. (2011). Organic condensation: A vital link connecting aerosol formation to cloud condensation nuclei (CCN) concentrations. *Atmos. Chem. Phys.*, (11):3865–3878.

Riipinen, I., Yli-Juuti, T., Pierce, J. R., Petäjä, T., Worsnop, D. R., Kulmala, M., and Donahue, N. M. (2012). The contribution of organics to atmospheric nanoparticle growth. *Nature Geosci*, 5(7):453–458.

Rovelli, G., Miles, R. E. H., Reid, J. P., and Clegg, S. L. (2016). Accurate Measurements of Aerosol Hygroscopic Growth over a Wide Range in Relative Humidity. *J. Phys. Chem. A*, 120(25):4376–4388.

Rovelli, G., Song, Y.-C., Maclean, A. M., Topping, D. O., Bertram, A. K., and Reid, J. P. (2019). Comparison of Approaches for Measuring and Predicting the Viscosity of Ternary Component Aerosol Particles. *Anal. Chem.*, 91(8):5074–5082.

Rumble, R, J., Lide, R, D., and Bruno, J, T. (2018). *CRC Handbook of Chemistry and Physics, 99th Ed.* CRC press, Taylor & Francis Group, Boca Raton, FL, 99 edition.

Saha, P. K. and Grieshop, A. P. (2016). Exploring Divergent Volatility Properties from Yield and Thermodenuder Measurements of Secondary Organic Aerosol from α-Pinene Ozonolysis. *Environ. Sci. Technol.*, 50(11):5740–5749.

Seinfeld, J. H. and Pandis, S. N. (2016). *Atmospheric Chemistry and Physics: From Air Pollution to Climate Change*. John Wiley & Sons.

Sheehan, P. E. and Bowman, F. M. (2001). Estimated Effects of Temperature on Secondary Organic Aerosol Concentrations. *Environ. Sci. Technol.*, 35(11):2129–2135.

Shiraiwa, M., Ammann, M., Koop, T., and Poschl, U. (2011). Gas uptake and chemical aging of semisolid organic aerosol particles. *Proc. Natl. Acad. Sci. U.S.A.*, 108(27):11003–11008.

Shiraiwa, M., Li, Y., Tsimpidi, A. P., Karydis, V. A., Berkemeier, T., Pandis, S. N., Lelieveld, J., Koop, T., and Pöschl, U. (2017). Global distribution of particle phase state in atmospheric secondary organic aerosols. *Nat. Commun.*, 8:15002.

Shiraiwa, M., Pfrang, C., Koop, T., and Pöschl, U. (2012). Kinetic multi-layer model of gas-particle interactions in aerosols and clouds (KM-GAP): Linking condensation,

evaporation and chemical reactions of organics, oxidants and water. *Atmos. Chem. Phys.*, 12(5):2777–2794.

Smith, J. N., Barsanti, K. C., Friedli, H. R., Ehn, M., Kulmala, M., Collins, D. R., Scheckman, J. H., Williams, B. J., and McMurry, P. H. (2010). Observations of aminium salts in atmospheric nanoparticles and possible climatic implications. *Proc. Natl. Acad. Sci. U.S.A.*, 107(15):6634–9.

Song, Y. C., Haddrell, A. E., Bzdek, B. R., Reid, J. P., Bannan, T., Topping, D. O., Percival, C., and Cai, C. (2016). Measurements and Predictions of Binary Component Aerosol Particle Viscosity. *J. Phys. Chem. A*, 120(41):8123–8137.

Stocker, T. F., Qin, D., Plattner, G.-K., Tignor, M., Allen, S. K., Boschung, J., Nauels, A., Xia, Y., Bex, V., Midgley, P. M., et al. (2013). *Climate Change 2013: The Physical Science Basis*. Cambridge University Press Cambridge.

Topping, D., Barley, M., Bane, M. K., Higham, N., Aumont, B., Dingle, N., and McFiggans, G. (2016). UManSysProp v1.0: An online and open-source facility for molecular property prediction and atmospheric aerosol calculations. *Geosci. Model Dev.*, 9(2):899–914.

Tsigaridis, K., Daskalakis, N., Kanakidou, M., Adams, P. J., Artaxo, P., Bahadur, R., Balkanski, Y., Bauer, S. E., Bellouin, N., Benedetti, A., Bergman, T., Berntsen, T. K., Beukes, J. P., Bian, H., Carslaw, K. S., Chin, M., Curci, G., Diehl, T., Easter, R. C., Ghan, S. J., Gong, S. L., Hodzic, A., Hoyle, C. R., Iversen, T., Jathar, S., Jimenez, J. L., Kaiser, J. W., Kirkevåg, A., Koch, D., Kokkola, H., Lee, Y. H., Lin, G., Liu, X., Luo, G., Ma, X., Mann, G. W., Mihalopoulos, N., Morcrette, J.-J., Müller, J.-F., Myhre, G., Myriokefalitakis, S., Ng, N. L., O'Donnell, D., Penner, J. E., Pozzoli, L., Pringle, K. J., Russell, L. M., Schulz, M., Sciare, J., Seland, Ø., Shindell, D. T., Sillman, S., Skeie, R. B., Spracklen, D., Stavrakou, T., Steenrod, S. D., Takemura, T., Tiitta, P., Tilmes, S., Tost, H., van Noije, T., van Zyl, P. G., von Salzen, K., Yu, F., Wang, Z., Wang, Z., Zaveri, R. A., Zhang, H., Zhang, K., Zhang, Q., and Zhang, X. (2014). The AeroCom evaluation and intercomparison of organic aerosol in global models. *Atmos. Chem. Phys.*, 14(19):10845–10895.

Ulbrich, I. M., Canagaratna, M. R., Zhang, Q., Worsnop, D. R., and Jimenez, J. L. (2009). Interpretation of organic components from Positive Matrix Factorization of aerosol mass spectrometric data. *Atmos. Chem. Phys.*, 9(9):2891–2918.

Vaden, T. D., Imre, D., Beránek, J., Shrivastava, M., and Zelenyuk, A. (2011). Evaporation kinetics and phase of laboratory and ambient secondary organic aerosol. *Proc. Natl. Acad. Sci. U.S.A.*, 108(6):2190–2195.

VandenBoer, T. C., Petroff, A., Markovic, M. Z., and Murphy, J. G. (2011). Size distribution of alkyl amines in continental particulate matter and their online detection in the gas and particle phase. *Atmos. Chem. Phys.*, 11(9):4319–4332.

Vesala, T., Kulmala, M., Rudolf, R., Vrtala, A., and Wagner, P. E. (1997). Models for condensational growth and evaporation of binary aerosol particles. *J. Aerosol Sci.*, 28(4):565–598.

Virtanen, A., Joutsensaari, J., Koop, T., Kannosto, J., Yli-Pirilä, P., Leskinen, J., Mäkelä, J. M., Holopainen, J. K., Pöschl, U., Kulmala, M., Worsnop, D. R., and Laaksonen, A. (2010). An amorphous solid state of biogenic secondary organic aerosol particles. *Nature*, 467(7317):824–827.

Wexler, A. S. and Clegg, S. L. (2002). Atmospheric aerosol models for systems including the ions H^+ , NH_4^+ , Na^+ , SO_4^{2-} , NO_3^- , Cl^- , Br^- , and H_2O. *J. Geophys. Res.*, 107(D14):4207.

Wilson, J., Imre, D., Beraek, J., Shrivastava, M., and Zelenyuk, A. (2015). Evaporation Kinetics of Laboratory-Generated Secondary Organic Aerosols at Elevated Relative Humidity. *Environ. Sci. Technol.*, 49(1):243–249.

Yang, X.-S. and Deb, S. (2009). Cuckoo Search via Lévy Flights. *India. IEEE Publications*, pages 210–214.

Yli-Juuti, T., Barsanti, K., Hildebrandt Ruiz, L., Kieloaho, A.-J., Makkonen, U., Petäjä, T., Ruuskanen, T., Kulmala, M., and Riipinen, I. (2013). Model for acid-base chemistry in nanoparticle growth (MABNAG). *Atmos. Chem. Phys*, 13:12507–12524.

Youn, J. S., Crosbie, E., Maudlin, L. C., Wang, Z., and Sorooshian, A. (2015). Dimethylamine as a major alkyl amine species in particles and cloud water: Observations in semi-arid and coastal regions. *Atmospheric Environ.*, 122:250–258.

Yu, H., Kaufman, Y. J., Chin, M., Feingold, G., Remer, L. A., Anderson, T. L., Balkanski, Y., Bellouin, N., Boucher, O., Christopher, S., DeCola, P., Kahn, R., Koch, D., Loeb, N., Reddy, M. S., Schulz, M., Takemura, T., and Zhou, M. (2006).

A review of measurement-based assessments of the aerosol direct radiative effect and forcing. *Atmos. Chem. Phys.*, 6(3):613–666.

Zhang, Q., Alfarra, M. R., Worsnop, D. R., Allan, J. D., Coe, H., Canagaratna, M. R., and Jimenez, J. L. (2005). Deconvolution and Quantification of Hydrocarbon-like and Oxygenated Organic Aerosols Based on Aerosol Mass Spectrometry. *Environ. Sci. Technol.*, 39(13):4938–4952.

Zhang, Q., Jimenez, J. L., Canagaratna, M. R., Allan, J. D., Coe, H., Ulbrich, I., Alfarra, M. R., Takami, A., Middlebrook, A. M., Sun, Y. L., Dzepina, K., Dunlea, E., Docherty, K., DeCarlo, P. F., Salcedo, D., Onasch, T., Jayne, J. T., Miyoshi, T., Shimono, A., Hatakeyama, S., Takegawa, N., Kondo, Y., Schneider, J., Drewnick, F., Borrmann, S., Weimer, S., Demerjian, K., Williams, P., Bower, K., Bahreini, R., Cottrell, L., Griffin, R. J., Rautiainen, J., Sun, J. Y., Zhang, Y. M., and Worsnop, D. R. (2007). Ubiquity and dominance of oxygenated species in organic aerosols in anthropogenically-influenced Northern Hemisphere midlatitudes. *Geophys. Res. Lett.*, 34(13).

Zhang, Q., Jimenez, J. L., Canagaratna, M. R., Ulbrich, I. M., Ng, N. L., Worsnop, D. R., and Sun, Y. (2011). Understanding atmospheric organic aerosols via factor analysis of aerosol mass spectrometry: A review. *Anal Bioanal Chem*, 401(10):3045–3067.

Zobrist, B., Marcolli, C., Pedernera, D. A., and Koop, T. (2008). Do atmospheric aerosols form glasses? *Atmos. Chem. Phys.*, 8(17):5221–5244.

Zuend, A., Marcolli, C., Luo, B. P., and Peter, T. (2008). A thermodynamic model of mixed organic-inorganic aerosols to predict activity coefficients. *Atmos. Chem. Phys.*, 8(16):4559–4593.

Zuend, A., Marcolli, C., Peter, T., and Seinfeld, J. H. (2010). Computation of liquid-liquid equilibria and phase stabilities: Implications for RH-dependent gas/particle partitioning of organic-inorganic aerosols. *Atmos. Chem. Phys.*, 10(16):7795–7820.